

GFDL SHIELD: A Unified System for Weather-to-Seasonal Prediction

Lucas Harris¹, Linjiong Zhou^{1,2}, Shian-Jiann Lin¹, Jan-Huey Chen^{1,3}, Xi Chen^{1,2}, Kun Gao^{1,2}, Matthew Morin^{1,3}, Shannon Rees^{1,3}, Yongqiang Sun^{1,2}, Mingjing Tong^{1,4}, Baoqiang Xiang^{1,3}, Morris Bender^{1,2}, Rusty Benson¹, Kai-Yuan Cheng^{1,2}, Spencer Clark^{1,5}, Oliver Elbert^{1,5}, Andrew Hazelton^{1,2*}, J. Jacob Huff^{1,3}, Alex Kaltenbaugh^{1,3}, Zhi Liang¹, Timothy Marchok¹, Hyeyum Hailey Shin^{1,3}, and William Stern¹

¹NOAA/Geophysical Fluid Dynamics Laboratory, Princeton, New Jersey.

²Cooperative Institute for Modeling the Earth System, Program in Oceanic and Atmospheric Sciences, Princeton University, Princeton, New Jersey.

³University Corporation for Atmospheric Research, Boulder, Colorado.

⁴SAIC, Princeton, New Jersey.

⁵Vulcan, Inc., Seattle, Washington.

Corresponding author: Lucas Harris (lucas.harris@noaa.gov)

*Current affiliation: NOAA/Atlantic Oceanographic and Meteorological Laboratory, Miami, Florida.

Key Points:

- A unified “one code, one executable, one workflow” global prediction modeling system is presented.
- SHIELD’s multiple configurations show prediction skill and simulation fidelity matching or exceeding those of existing models.
- The FV3 Dynamical Core provides a powerful foundation for unified prediction modeling.

23 Abstract

24 We present the System for High-resolution prediction on Earth-to-Local Domains (SHiELD), an
25 atmosphere model coupling the nonhydrostatic FV3 Dynamical Core to a physics suite originally
26 taken from the Global Forecast System. SHiELD is designed to demonstrate new capabilities
27 within its components, explore new model applications, and to answer scientific questions
28 through these new functionalities. A variety of configurations are presented, including short-to-
29 medium-range and subseasonal-to-seasonal (S2S) prediction, global-to-regional convective-scale
30 hurricane and contiguous US precipitation forecasts, and global cloud-resolving modeling.
31 Advances within SHiELD can be seamlessly transitioned into other Unified Forecast System
32 (UFS) or FV3-based models, including operational implementations of the UFS.

33 Continued development of SHiELD has shown improvement upon existing models. The flagship
34 13-km SHiELD demonstrates steadily improved large-scale prediction skill and precipitation
35 prediction skill. SHiELD and the coarser-resolution S-SHiELD demonstrate a superior diurnal
36 cycle compared to existing climate models; the latter also demonstrates 28 days of useful
37 prediction skill for the Madden-Julian Oscillation. The global-to-regional nested configurations
38 T-SHiELD (tropical Atlantic) and C-SHiELD (contiguous United States) shows significant
39 improvement in hurricane structure from a new tracer advection scheme and promise for
40 medium-range prediction of convective storms, respectively.

41 Plain Language Summary

42 At many weather forecasting centers where computer weather models are run, different models
43 are run for different applications. However, each separate model multiplies the effort needed to
44 maintain and upgrade each model and makes it difficult to move improvements between models.

45 We present a new “unified” weather modeling system, SHiELD, able to be configured for a
46 variety of applications. This system uses a powerful computer code, FV3, to compute the fluid
47 motion of the atmosphere at any scale, and also able to zoom in on areas of interest to better
48 “see” severe storms or intense hurricanes. We show how we started from a quickly-assembled
49 model for testing FV3 and then gradually improved the representation of different atmospheric
50 processes and expanded into new uses for the system, including short-range severe thunderstorm
51 prediction, hurricane forecasting, and forecasts out to as long as six weeks. We address some of
52 the challenges that we faced and discuss prospects for future model improvements. Since many
53 of the parts of SHiELD are used by models being developed by the National Weather Service for
54 use by weather forecasters, the advances described here can be rapidly introduced into those
55 models, eventually improving official forecasts.

56

57

58 **1 Unified Modeling at GFDL**

59 As computing power increases global atmosphere models are now capable of regular
60 simulation at resolutions that had been the sole domain of regional atmospheric models. The
61 Integrated Forecast System (IFS; ECMWF 2019a,b) of the European Center for Medium-Range
62 Weather Forecasting (ECMWF) runs on a 9-km grid, and the Global Forecast System (GFS;
63 Sela2010) of the US National Centers for Environmental Prediction (NCEP) runs on a 13-km
64 grid. Some IPCC-class climate models now use grids with spacings as fine as 25 km (Chen and
65 Lin 2013; Vecchi et al. 2019; Haarsma et al. 2017). Global atmosphere models lack the lateral
66 boundary errors that contaminate the solutions of regional models after a few days of simulation.
67 They thus allow us to extend mesoscale and storm-scale predictions into the medium range and
68 beyond (Harris and Lin 2013, 2014; Zhou et al. 2019; Harris et al. 2019). Global modeling also
69 brings many new challenges—one cannot “throw your garbage in the neighbor’s yard” in global
70 modeling, so to speak. Biases and radiative imbalances must be minimized, as must errors
71 *anywhere* in the atmosphere that could potentially grow and contaminate the entire domain.

72 A unified modeling system supports a variety of applications at a wide range of spatial
73 and temporal scales within a single framework. These systems promise to simplify operational
74 and research modeling suites and better exchange improvements and bug fixes between
75 applications. The Unified Model of the United Kingdom Met Office (UKMO; Brown et al. 2012)
76 is the most notable unified system. Variable-resolution models (Harris and Lin 2014, McGregor
77 2015) are particularly well-suited for unified modeling as they can efficiently reach very high
78 resolutions over part of the earth, replacing the highest-resolution regional models (Hazelton et
79 al. 2018a,b, Zhou et al. 2019) and potentially extending their lead times.

80 Here at GFDL a hierarchy of models has been developed for a variety of time and space
81 scales, from centennial-scale earth-system simulations (Dunne et al. 2020) to very high-
82 resolution weather prediction. The GFDL suite is unified around a single dynamical core, the
83 GFDL Finite-Volume Cubed-Sphere Dynamical Core (FV3, or FV³; Putman and Lin 2007), and
84 a single framework, the Flexible Modeling System (FMS; Balaji 2012), and other shared
85 components. We describe one part of this suite, the System for High Resolution Prediction on
86 Earth-to-Local Domains, or SHiELD. This model, previously called fvGFS, was developed as a
87 prototype of the Next-Generation Global Prediction System (NGGPS) of the National Weather
88 Service, and of the broader Unified Forecast System (UFS). SHiELD continues GFDL’s high-
89 resolution global modeling program previously established using the High-Resolution
90 Atmosphere Model (HiRAM; Zhao et al. 2009; Chen and Lin 2013). SHiELD couples the
91 nonhydrostatic FV3 dynamical core (Lin et al. 2017) to a physics suite originally from the GFS
92 (Han et al. 2017 and references therein) and the Noah Land Surface Model (Ek et al. 2002).
93 SHiELD can be used for a variety of timescales but has been designed with a particular focus on
94 short-to-medium range weather (18 hours to 10 days) and into the subseasonal to seasonal (S2S;
95 several weeks to several months) range. Seasonal to decadal predictions and centennial-scale
96 climate projections coupled to a dynamical ocean are performed at GFDL using the Seamless
97 System for Prediction and Earth System Research (SPEAR, Delworth et al. 2020), the Coupled
98 Model version 4 (CM4; Held et al. 2020), and the Earth System Model version 4 (ESM4, Dunne
99 et al. 2020).

100 Since FV3 is designed to adapt to a variety of purposes and to any scale of atmospheric
101 motion it is an ideal platform for a unified modeling system. All of the SHiELD configurations
102 described here, as well as regional and doubly-periodic applications lying beyond the scope of
103 this paper, use the same code base, the same executable, the same preprocessor, the same
104 runscripts, and same post-processing tools, demonstrating a true unification for modeling on
105 weather-to-S2S timescales. This approach also suggests how further unification with GFDL’s
106 climate models, which use a different atmospheric physics (Zhao et al. 2018), the MOM6
107 Dynamical Ocean (Adcroft et al. 2019), and the GFDL LM4 land model (Shevliakova et al.
108 2020), may proceed. Advances in SHiELD can be seamlessly moved into other UFS models,
109 including the 2019 upgraded GFSv15, and other FV3-based models. Most notably, advances in
110 SHiELD can migrate into UFS models slated for operational implementation at NCEP, including
111 the FV3-based GFSv15. NASA GEOS (Putman and Suarez 2017), NASA/Harvard GEOS-Chem
112 High-Performance (GHCP), CESM-FV3, and the Chinese Academy of Sciences’ F-GOALS all
113 also use FV3 as their dynamical core and can benefit from the advances described below. This
114 diversity of FV3-based models shows the advantages of using common components to leverage
115 advances in the dynamical core but while still allowing centers to tailor their models to their own
116 needs, the freedom to innovate new model designs, and to encourage the development of models
117 as holistic integrated systems, rather than clumsily joining independent components.

118 SHiELD is designed for exploratory research into model design and development, with a
119 focus on dynamics and physics-dynamics integration, and for research on prediction and
120 atmospheric processes on timescales from a few hours to a few months. SHiELD is currently
121 focused on deterministic prediction although effective S2S prediction will require the
122 development of a simple ensemble (cf. Chen and Lin 2013).

123 The design, evolution, configurations, and simulation characteristics of SHiELD are the
124 subject of this paper. Section 2 describes the components of SHiELD and how they work
125 together as a complete modeling system. Section 3 describes the four configurations of SHiELD
126 for a variety of applications, including medium-range weather, continental convection, tropical
127 meteorology and hurricanes, and S2S prediction. Section 4 summarizes the history of SHiELD
128 development and discusses prospects for future work.

129 **2 SHiELD Components**

130 **2.1 Nonhydrostatic FV3 Dynamical Core**

131 All SHiELD simulations use the nonhydrostatic solver within the FV3 Dynamical Core.
132 This core has been described in detail in other papers (Lin 2004, Putman and Lin 2007, Harris
133 and Lin 2013, and references therein) and will only be summarized here. FV3 solves the fully-
134 compressible Euler equations on the gnomonic cubed-sphere grid and a Lagrangian vertical
135 coordinate. Fast vertically-propagating sound and gravity waves are solved by the semi-implicit
136 method; otherwise the algorithm is fully explicit. FV3 advances sound and gravity wave
137 processes and advects thermodynamic variables on the shortest “acoustic” timestep, while sub-
138 cycled tracer advection and vertical remapping (cf. Lin 2004) are performed on an intermediate
139 “remapping” timestep, in turn performed multiple times per physics timestep.

140 FV3’s discretization along Lagrangian surfaces uses the piecewise-parabolic method,
141 which previously used a monotonicity constraint to ensure positivity and to dissipate energy
142 cascading to grid scale. In nonhydrostatic FV3 dynamical quantities (vorticity, potential

143 temperature, and air mass) are advected by a non-monotonic scheme to reduce dissipation of
144 resolved-scale modes. Previous work with nonhydrostatic FV3 had continued to use a monotonic
145 advection scheme to avoid unphysical negative values. In this manuscript we present results
146 using a new *positive-definite* but non-monotonic scheme to advect tracers, which greatly
147 improves the representation of marginally-resolved and discontinuous features without creating
148 computational noise at sharp gradients. This scheme is described in detail in Appendix A and
149 applications to the representation of tropical cyclones in section 3d.

150 2.2 GFS/SHiELD Physics and Noah LSM

151 SHiELD inherits the [GFS suite of physical parameterizations developed by the](#)
152 [Environmental Modeling Center \(EMC\) of NCEP \(2020\)](#). The initial 2016 version of SHiELD,
153 implemented for dynamical core testing during Phase II of NGGPS, used physics largely
154 identical to the then-operational GFSv13: The Simplified Arakawa-Schubert (SAS) shallow and
155 deep convection schemes described in Han and Pan (2011); the hybrid Eddy-diffusivity Mass-
156 flux (EDMF) scheme (Han et al. 2016); the Rapid Radiative Transfer Model (RRTM; Clough et
157 al. 2005); the microphysics of Zhao and Carr (1997) and cloud-fraction scheme of Xu and
158 Randall (1996); the Navy's simplified ozone scheme (McCormack et al. 2006); and the GFS
159 orographic gravity wave drag and mountain blocking schemes (Alpert 2002) and convective
160 gravity wave drag scheme of Chun and Baik (1998).

161 We have since made many changes to the physics to be able to support new applications,
162 especially for convective scale prediction and marine phenomena, or to take advantage of new
163 capabilities within the FV3 dynamical core. We first introduced the six-category GFDL
164 microphysics and cloud fraction scheme (Zhou et al. 2019) with the fast microphysical processes
165 split out of the physics driver and taking place on the shorter remapping timestep. Later, the
166 GFDL microphysics was fully integrated within FV3 (see appendix B). Several new PBL
167 schemes have also been used in SHiELD, including a modified hybrid EDMF PBL as per Zhang
168 et al. 2015, and the Yonsei University scheme (YSU; Hong et al. 2006, Hong 2010, Wilson and
169 Fovell 2018). We have also adopted the Scale-Aware SAS (Han et al. 2017) convection scheme
170 in more recent versions of SHiELD.

171 The land surface model (LSM) is the Noah land-surface model (Ek et al. 2003),
172 integrated within the physics and paired to the GFS surface-layer scheme. In 2017 Noah was
173 upgraded to use the high-resolution land surface data (Wei et al. 2017), which greatly improves
174 the appearance of land-surface fields in convective-scale simulations.

175 2.3 Mixed-layer Ocean

176 Initially sea-surface temperatures (SSTs) were prescribed as the climatological SST plus
177 an SST anomaly from initial conditions which gradually decays to zero, without influence from
178 the atmosphere. However, air-sea interactions are critical for several phenomena of interest to us,
179 especially tropical cyclones and the Madden-Julian Oscillation (MJO) and may impact large-
180 scale skill as well. To incorporate atmosphere-ocean interaction, we have implemented a
181 modification of the mixed-layer ocean (MLO) of Pollard et al. 1973. This simple ocean computes
182 the mixed layer depth and heat within that mixed layer as prognostic variables, with tendencies
183 computed from the net surface heat flux. The SST is nudged towards the NCEP Real-Time
184 Global Sea Surface Temperature (RTGSST; Thiébaux et al. 2003) climatology plus a fixed initial
185 anomaly which decays with a fixed timescale. The ocean mixed layer depth is also nudged

186 toward observed climatology (de Boyer Montégut et al., 2004). While considerably simpler than
187 the three-dimensional dynamical oceans in CM4 (Held et al. 2020) and in the GFDL Hurricane
188 Model (Bender et al. 2019), the MLO still represents the thermodynamic and dynamic ocean
189 interactions of greatest significance on the timescales for which SHiELD is used (Hazelton et al.
190 2018b), without incurring the complexity of a three-dimensional dynamical ocean.

191 2.4 Interoperability with other UFS models

192 SHiELD was designed to work with other models that use FV3, FMS, the GFS Physics
193 Driver, and/or the Interoperable Physics Driver ([IPD](#)). The IPD is the interface between FV3 and
194 the GFS Physics Driver, although it can support other physics suites. Innovations within
195 SHiELD can then be seamlessly exchanged with other models using these same components. For
196 example, the transition of FV3 and the GFDL Microphysics into the operational GFSv15 was
197 accelerated by the IPD. Conversely, schemes which have been introduced into the GFS Physics
198 Driver by the broader community can then be integrated into SHiELD, including the numerous
199 schemes implemented by Zhang et al. (2018).

200 3 SHiELD Configurations

201 SHiELD leverages the flexibility of FV3 to be able to make accurate and efficient
202 simulations at a variety of spatial and temporal scales. Much of the development of SHiELD
203 (and previously, of HiRAM) has been driven by a desire to improve the simulation quality at the
204 convection-permitting resolutions covered by the range of SHiELD configurations.

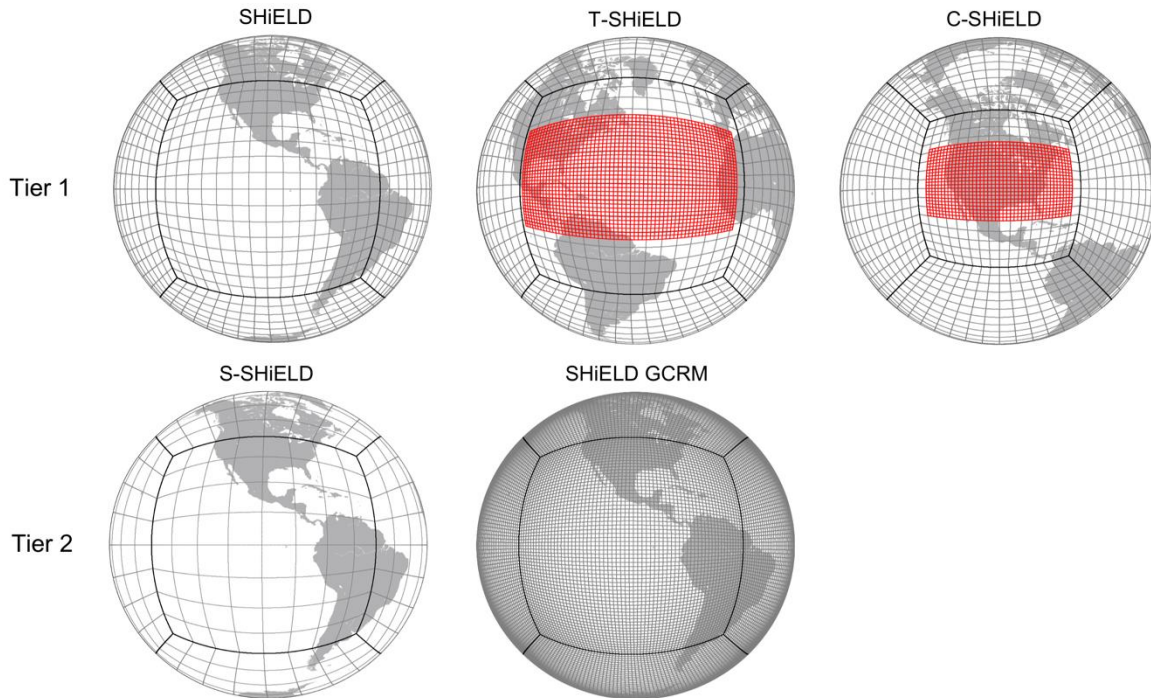
205 We present four different configurations of SHiELD. All configurations are global
206 domains using either a uniform grid or a locally refined grid using nesting or stretching (Harris
207 and Lin 2013; Harris et al. 2016; Zhou et al. 2019). SHiELD can also run on FV3's doubly-
208 periodic domain (Held and Zhou, 2006, Arnold and Putman, 2018) or on a regional domain using
209 any regular quadrilateral grid (Dong et al., 2020), at spatial resolutions down to a few tens of
210 meters (Jeevanjee 2017). These applications lie beyond the scope of this paper.

211 The four configurations can be fit within two “tiers”; Tier-1 configurations are the most
212 well-tested, having originally been developed as prototypes to replace legacy NCEP models by
213 FV3-based UFS systems, and having been run in near-real time for several years. These
214 configurations demonstrate the capabilities of SHiELD, allow direct comparison to existing
215 operational models, and provide robust tests of the forecast skill and reliability of SHiELD.
216 Current real-time configurations are run twice daily and displayed at
217 <https://shield.gfdl.noaa.gov/>.

218 The Tier-1 configurations are our flagship 13-km SHiELD, a prototype for the now-
219 operational GFSv15 and for future upgrades of the GFS; (Tropical) T-SHiELD with a static, 3-
220 km nest spanning the tropical North Atlantic, a prototype of the Hurricane Analysis and Forecast
221 System (HAFS); and (Continental) C-SHiELD with a 3-km nest over the contiguous United
222 States (CONUS), a prototype of the Regional Forecast System (RFS). Each of the Tier-1
223 configurations are usually refreshed every year with a new version, indicated by the year of the
224 upgrade.

225 Our Tier-2 configurations address new challenges for numerical prediction and are still
226 under development. Our 25-km (Subseasonal) S-SHiELD addresses the challenging domain of
227 S2S prediction. Another configuration not discussed in this paper is the SHiELD global cloud-

228 resolving model (GCRM) and addresses the frontier computational and data challenges of such
 229 simulations. This configuration was submitted to the DYNAMICS of the Atmospheric general
 230 circulation Modeled On Non-hydrostatic Domains (DYAMOND) intercomparison (Stevens et al.
 231 2019, Satoh et al. 2019). Both configurations inspire the development of new functionality and
 232 capabilities within SHiELD and readily expose instabilities, climate drift, conservation issues,
 233 and other shortcomings. The advances driven by work on these frontier challenges help improve
 234 the Tier-1 configurations, demonstrating the value of a seamless prediction system. The domains
 235 for each of the four configurations plus the GCRM configuration are depicted schematically in
 236 Figure 1.



237

238 **Figure 1.** Current SHiELD configurations. Each plotted cell is 48x48 actual grid cells. Heavy
 239 black lines represent cubed-sphere edges; red lines represent nested grids. Note that the global
 240 domain of C-SHiELD (top center) is slightly stretched as per Harris2019.

241 Although all configurations follow the unified “one code, one executable, one workflow”
 242 structure of SHiELD, the configurations are not identical owing to the need to tailor each
 243 configuration for its specific application. Further, given the rapid pace of SHiELD development
 244 and the staggered development cycle for some of the configurations, we do not expect all of the
 245 Tier-1 configurations to always have the very latest developments. The development paths of the
 246 different SHiELD configurations can be seen in Table 1.

Configuration	SHiELD				T-SHiELD		C-SHiELD			S-SHiELD
Version	2016	2017	2018	2019	2017	2018	2017	2018	2019	2019
Resolution	13 km (c768)				13 km (c768) + 3-km nest (2880 x 1536)		20-to-9 km stretched (c768r15) + 3-km 3x nest (2016 x 1080)			25-km
Grid Cells	3.54 M				3.54 M + 4.23 M		3.54 M + 2.18 M			885 K
Vertical Levels	63	63	91	91	63	63	63	63	63	91
Physics Timestep	225	150	150	150	90	90	90	90	90	450
Remapping, Tracer, and MP Timestep	112.5	150	150	150	90/22.5	90/22.5	90/22.5	90/22.5	90/22.5	225
Acoustic Timestep	18.75	18.75	18.75	18.75	12.8/4.5	12.8/4.5	12.8/4.5	12.8/4.5	12.8/4.5	28.125
Tracer Advection Scheme	Monotonic	Monotonic	Pos. Def	Pos. Def	Monotonic	Pos. Def	Monotonic	Pos. Def	Pos. Def	Pos. Def
Microphysics	Zhao-Carr	Split GFDL	Inline GFDL	Inline GFDL	Split GFDL	Split GFDL	Split GFDL	Inline GFDL	Inline GFDL	Inline GFDL
PBL Scheme	Hybrid EDMF	Hybrid EDMF	YSU	YSU	Mod. EDMF	YSU	Mod. EDMF	YSU	YSU	YSU
Deep Convection Scheme	SAS	SA-SAS	SA-SAS	SA-SAS	SAS	SA-SAS	None	None	None	SAS
Ocean Surface	Specified	Specified	MLO	MLO	Specified	MLO	Specified	Specified	MLO	MLO

248 **Table 1.** Development of the four SHiELD configurations and their yearly revisions described in
249 this paper. Timesteps are given in seconds; for nested simulations the format is global/nested
250 timesteps. All configurations and versions use the same Noah LSM and RRTM, and all use SAS
251 or SA-SAS shallow convection except 2017 and 2018 C-SHiELD.

252 All configurations are initialized using the real-time GFS analyses made available by
253 NCEP following Chen et al. (2018). This “cold starting” from the hydrostatic, spectral GFS
254 could potentially leave the convective-scale configurations (T-SHiELD, C-SHiELD) at a
255 comparative disadvantage to models with native, specialized convective-scale data assimilation.
256 This issue is minimized here due to the ability of FV3-based models to “spin up” their
257 convective scales within a few hours of initialization and experience little degradation thereafter
258 (Hazelton et al. 2018a,b; Marchok et al. 2018; Zhang et al. 2018; Harris et al. 2019).

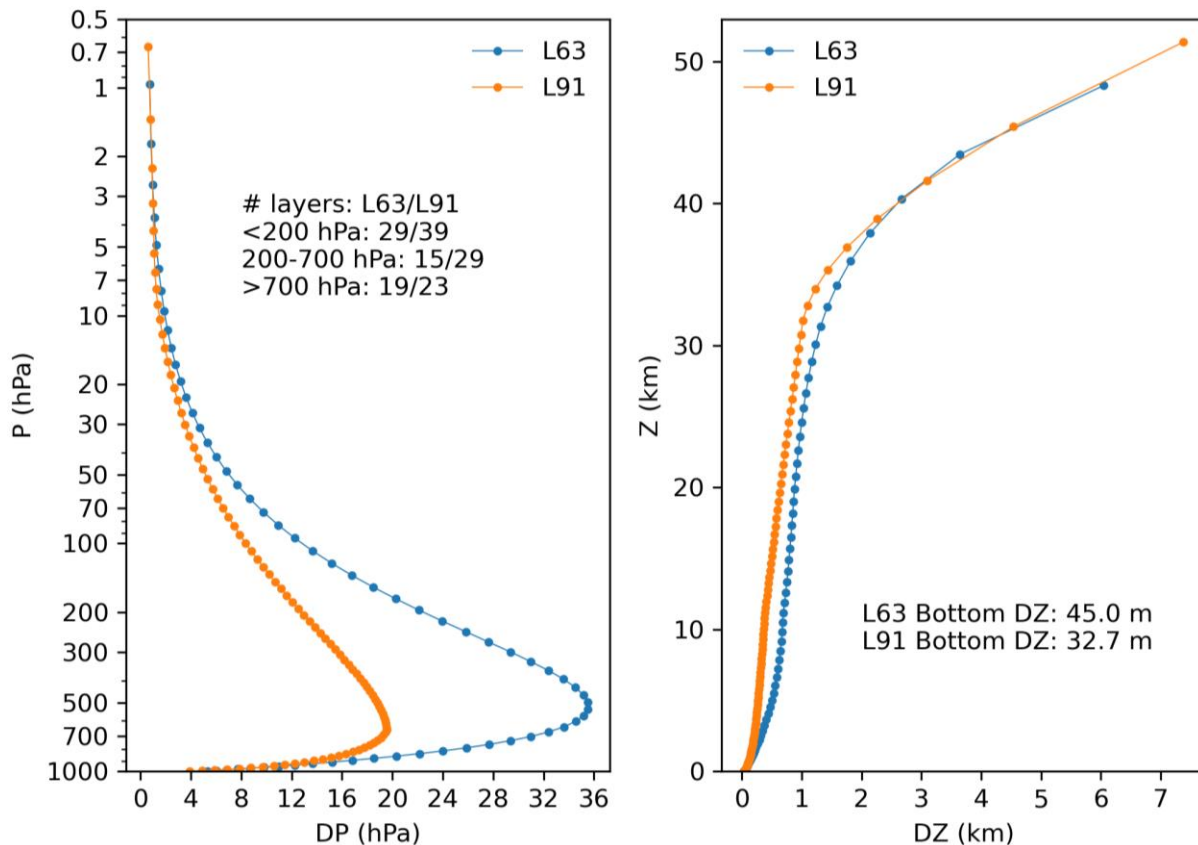
259 Computational efficiency is crucial for useful simulation modeling, for both real-time and
260 experimental applications. We present the timings for the most recent iterations of SHiELD in
261 Table 2. The 13-km SHiELD needs only 3096 processor cores to complete one day in under 8.5
262 minutes, the threshold traditionally used for operational global prediction. The 25-km S-SHiELD
263 completes 1.5 years per day with just over 1700 cores. C-SHiELD is necessarily more expensive
264 owing to its nested grid but still completes a five-day simulation in under two hours on less than
265 3500 cores. T-SHiELD has a nested grid with twice as many columns as C-SHiELD but is only
266 about 30% more expensive.

267 SHiELD is compiled with mixed-precision arithmetic: the dynamics (and the inlined
268 components of the microphysics) use single-precision arithmetic while the physics uses double-
269 precision. This differs from the practice used for most operational models (GFSv15 excluded)

270 and for GFDL climate models, which use double-precision arithmetic throughout. Tests with the
 271 2016 version of SHiELD had found no detectable difference in skill between predictions using
 272 mixed-precision and double-precision arithmetic.

273 2.1 SHiELD Medium-Range Weather Prediction

274 The flagship SHiELD configuration is designed for medium-range prediction with lead
 275 times of 24 hours to ten days. The design of SHiELD is similar to the operational GFS: a global
 276 c768 grid—a cubed-sphere with each face having 768 x 768 grid cells—with an average grid-cell
 277 width of about 13-km. The 2016 and 2017 versions of SHiELD used 63 vertical levels (Figure
 278 2), the same as the hydrostatic GFSv14 but with the uppermost semi-infinite layer removed to
 279 permit nonhydrostatic simulation. Starting in 2018, SHiELD increased the number of vertical
 280 levels to 91, increasing the number of vertical levels below 700 mb from 19 to 23 and decreasing
 281 the depth of the lowest model layer from 45 to 33 m.



282

283 **Figure 2.** Distribution of vertical levels in various SHiELD configurations for a surface pressure
 284 of 1000 hPa and a standard atmospheric temperature structure.

285 The simulation characteristics and prediction skill of SHiELD have been previously
 286 discussed in several papers and will not be repeated here. Improving predictions of tropical
 287 cyclone track, intensity, and genesis has been a key driver of SHiELD development: Chen et al.
 288 (2019a) describes the 2016 and 2017 versions, while the considerably improved 2018 version is
 289 described in Chen et al. (2019b). Most notably SHiELD greatly improves upon other global

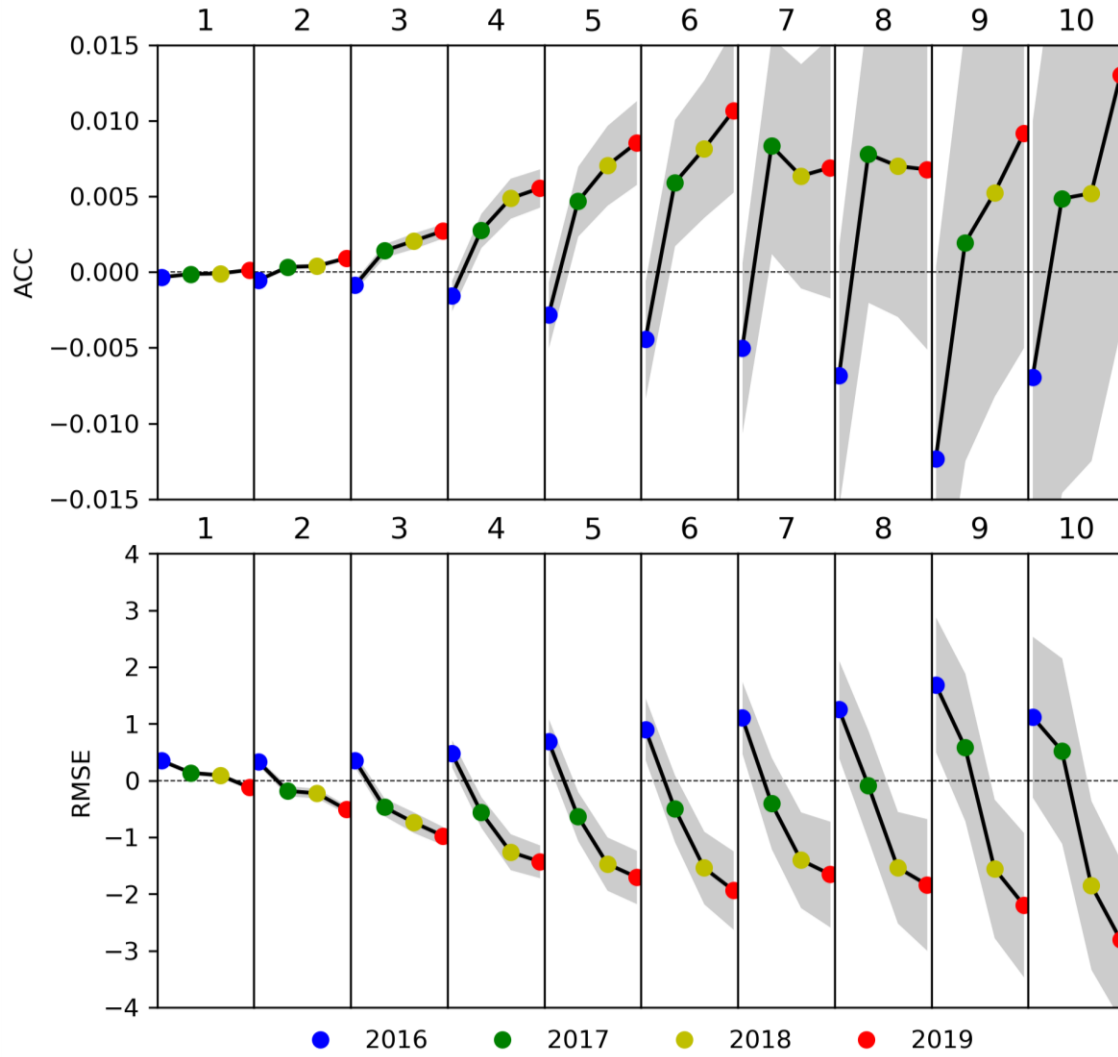
290 models' ability to predict tropical cyclone intensity. The large-scale prediction skill, and CONUS
291 precipitation and 2-m temperature skill, are briefly described for the 2016 and 2017 versions in
292 LZhou2019 and Harris2019.

293 The anomaly correlation coefficient (ACC) of the 500-mb geopotential height field is the
294 standard means for evaluating the large-scale prediction skill of medium-range prediction
295 models. Figure 3 (top) shows that the global ACC of SHiELD has been better at all lead times
296 than the contemporary GFS since the 2017 version, and significantly so on days 1–6. At all lead
297 times except for days 7 and 8, each new version has improved upon the previous version. The
298 result for root-mean square error (RMSE; Figure 3, bottom) is even more striking: every version
299 is an improvement upon the previous at every lead time, and both the 2018 and 2019 versions are
300 significantly better than the operational GFS. Results for just the northern hemisphere (20N--
301 80N, Supplemental Figure S1) are less dramatic but SHiELD still shows statistically significant
302 improvements in ACC and RMSE out to day 5. Both the GFS and all versions of SHiELD reach
303 an ACC of 0.6 at 8.3–8.5 days globally and 8.5–8.7 days in the northern hemisphere, with some
304 year-to-year and version-to-version variability.

305 The time series of day-5 global ACC and RMSE (Figure 4) shows that while there is a
306 general secular improvement in both SHiELD and the GFS, there can be large seasonal and even
307 interannual variability in forecast skill. Usually, predictions are more skillful in northern winter,
308 as strong synoptic forcing dominates the large-scale weather patterns, but some northern
309 summers see little to no forecast degradation. [The implementation of GFSv13 on 11 May 2016](#),
310 which included a major upgrade to the data assimilation cycling system of the GFS, significantly
311 reduced RMSE in May and June 2016 compared to the preceding four months of the year. These
312 results are worthy of further investigation. We do conclude that it may be misleading to use a
313 short time period to evaluate or compare global prediction models.

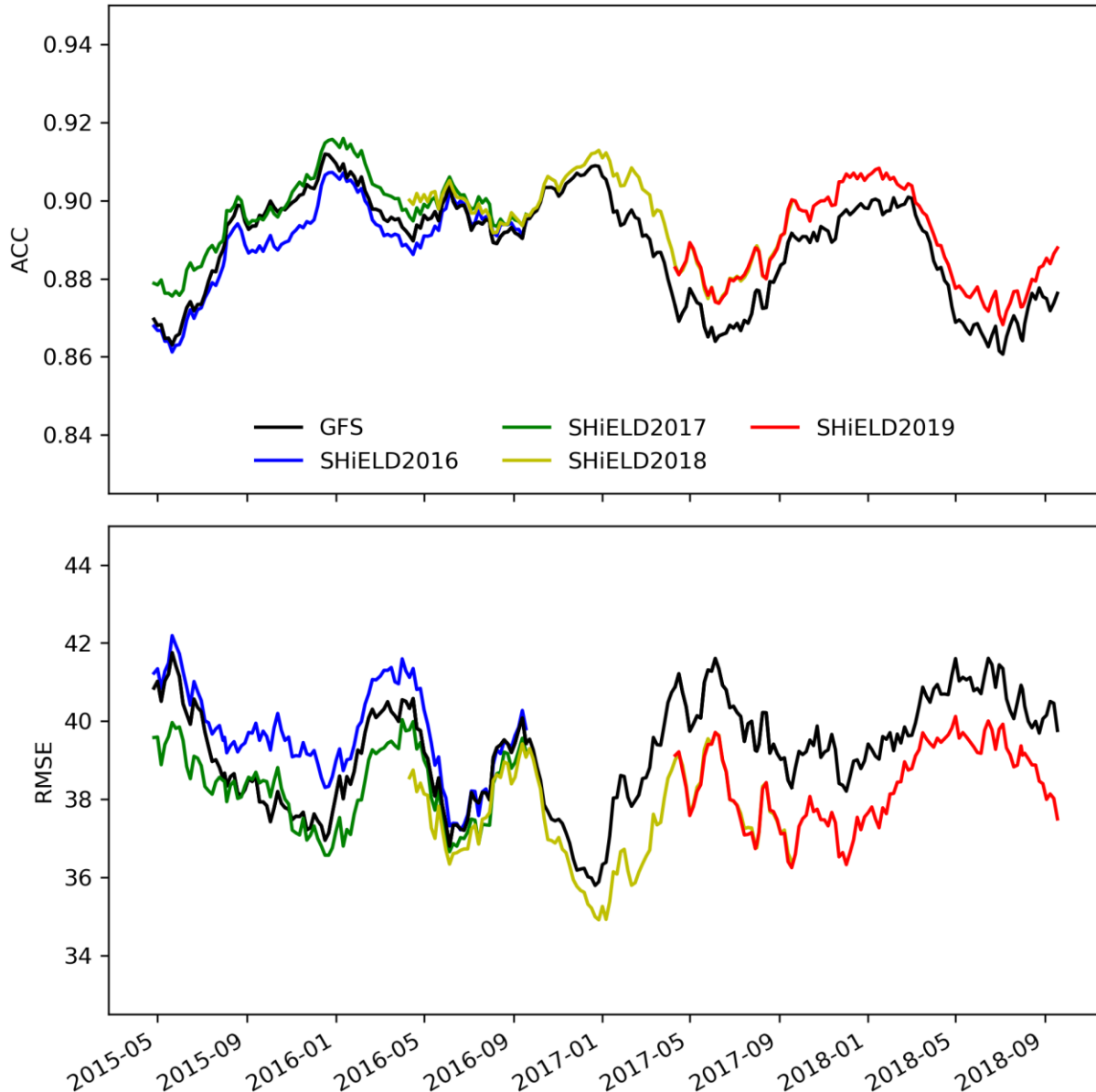
314 The time-evolution of the large-scale forecast skill for both the GFS and SHiELD are
315 very similar on monthly and shorter time-periods, which is expected as they use identical initial
316 conditions, and SHiELD benefits from continual upgrades of the GFS initial conditions. As
317 discussed in Chen et al. (2019b) the quality of the initial conditions is the preeminent factor in
318 determining the forecast skill for the large-scale circulation as well as for metrics such as
319 hurricane track forecasts that depend closely on the prediction skill of the large-scale flow.

320 These results are for hindcasts but the ACC and RMSE for our real-time forecasts are
321 nearly identical. An important caveat is that the operational GFS supports nearly the entire
322 NCEP modeling suite, and so the GFS has many more demands and a much more stringent
323 evaluation process imposed upon its development than does SHiELD. The development cycle of
324 the GFS will therefore necessarily be less rapid and more methodological than that of SHiELD.
325 Alternately, an experimental research model like SHiELD does have the freedom to pursue many
326 different avenues for model development (“failure is always an option”) so that the most
327 successful new ideas can later be transitioned into operations, a major goal of the UFS.



328

329 **Figure 3.** Global 500-mb geopotential height ACC (top) and RMSE (bottom, m) as a function of
 330 lead time for each version of the 13-km SHIELD, relative to the contemporary GFS. Gray
 331 shading is the 95% confidence interval. See Figure 4 for the time periods being compared here.

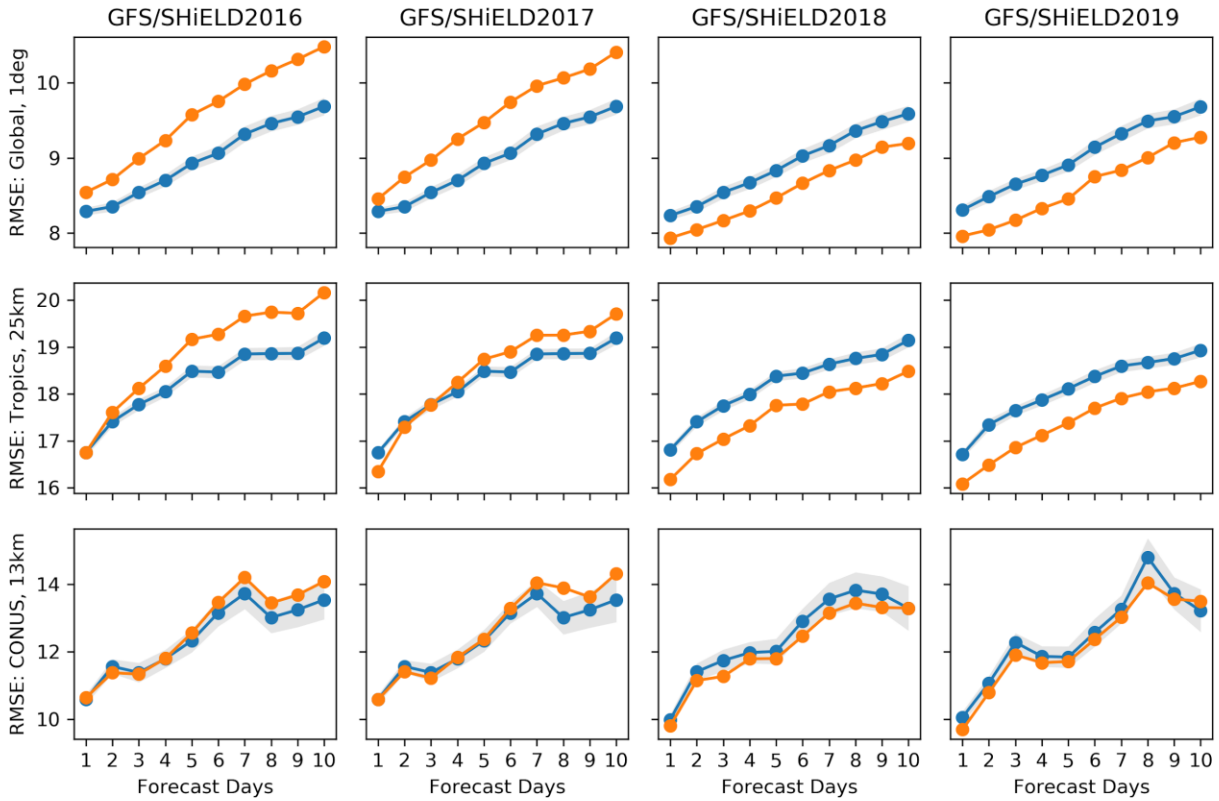


332

333 **Figure 4.** Smoothed time series of global 500-mb geopotential height ACC (top) and RMSE
 334 (bottom, m) at day 5 for each version of the 13-km SHIELD and the contemporary operational
 335 GFS. Note that the operational GFS upgraded to v13 on 11 May 2016 and v14 on 19 July 2017.

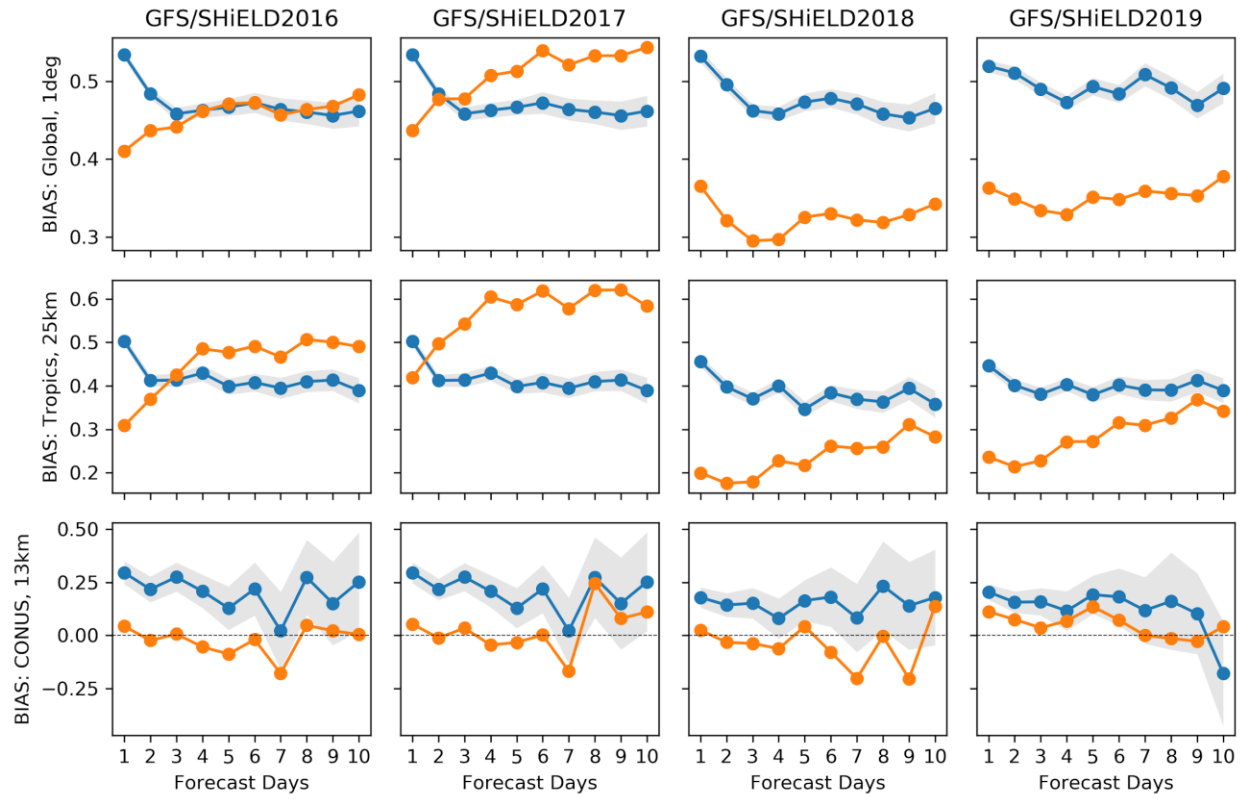
336 Precipitation RMSE and biases have also improved during SHIELD development. The
 337 2018 version significantly reduced both RMSE (Figure 5) and Bias (Figure 6) at all lead times
 338 compared to earlier versions. Prediction of CONUS precipitation is more challenging given the
 339 smaller area and larger seasonal cycle but RMSE still improves every year and there is nearly no
 340 bias, especially in the 2019 version. Zhou et al (2019) give a more thorough description of
 341 precipitation forecast skill, including other metrics. Probability distribution functions (PDFs) of
 342 precipitation (Figure 7) show that all of the versions depicted here have a low bias in the
 343 frequency of moderate precipitation and a high bias of both light and heavy precipitation rates

344 compared to TRMM, although versions of SHiELD using the GFDL microphysics (2017 and
345 later) modestly alleviate these biases. Both the GFS and all versions of 13-km SHiELD capture
346 the observed CONUS PDF very well.



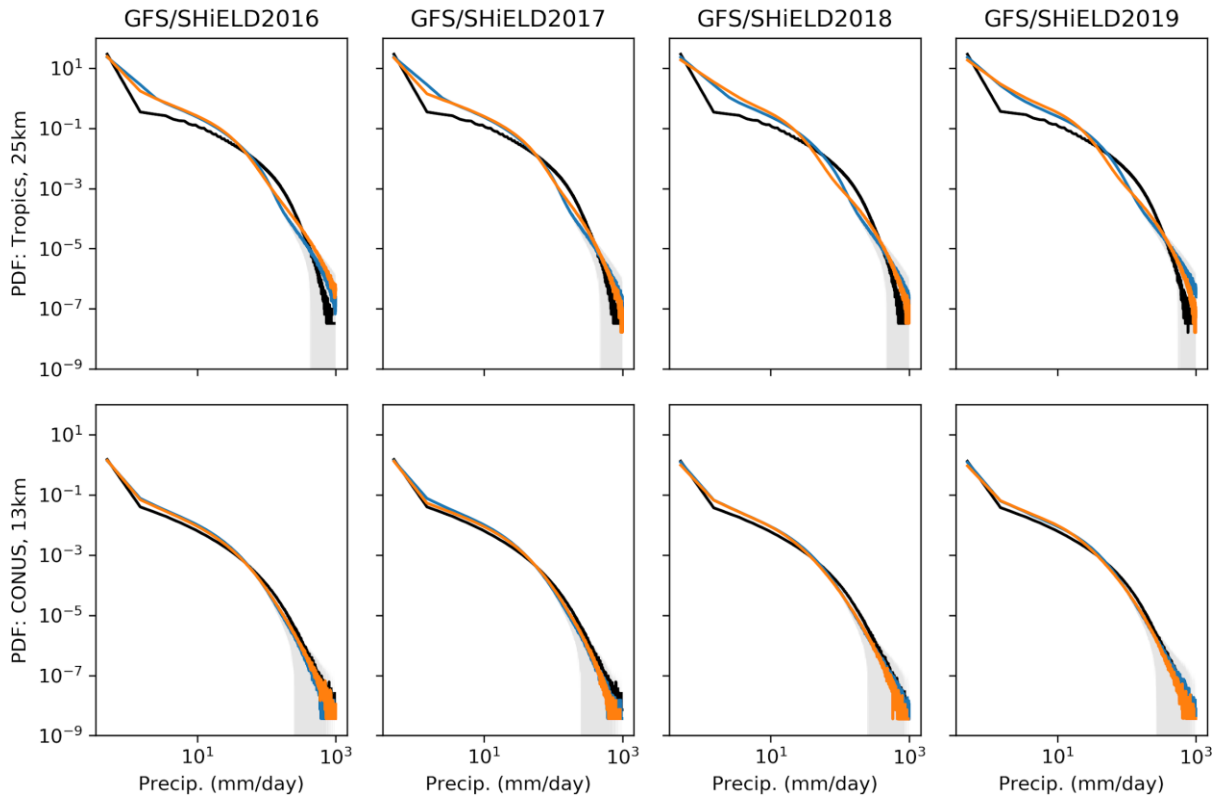
347

348 **Figure 5.** RMSE of 24-hour precipitation (mm) for different versions of 13-km SHIELD
 349 (orange) compared to contemporary GFS (blue). Each version's results are aggregated over the
 350 forecasts plotted in Figure 4. Top row: Global verification vs. GPCP dataset (regridded to 1
 351 degree); middle row: tropics (30S--30N) verification vs. TRMM dataset (regridded to 25 km);
 352 bottom row: CONUS verification vs. StageIV dataset (regridded to 13 km). Gray shading is the
 353 95% confidence interval.



354

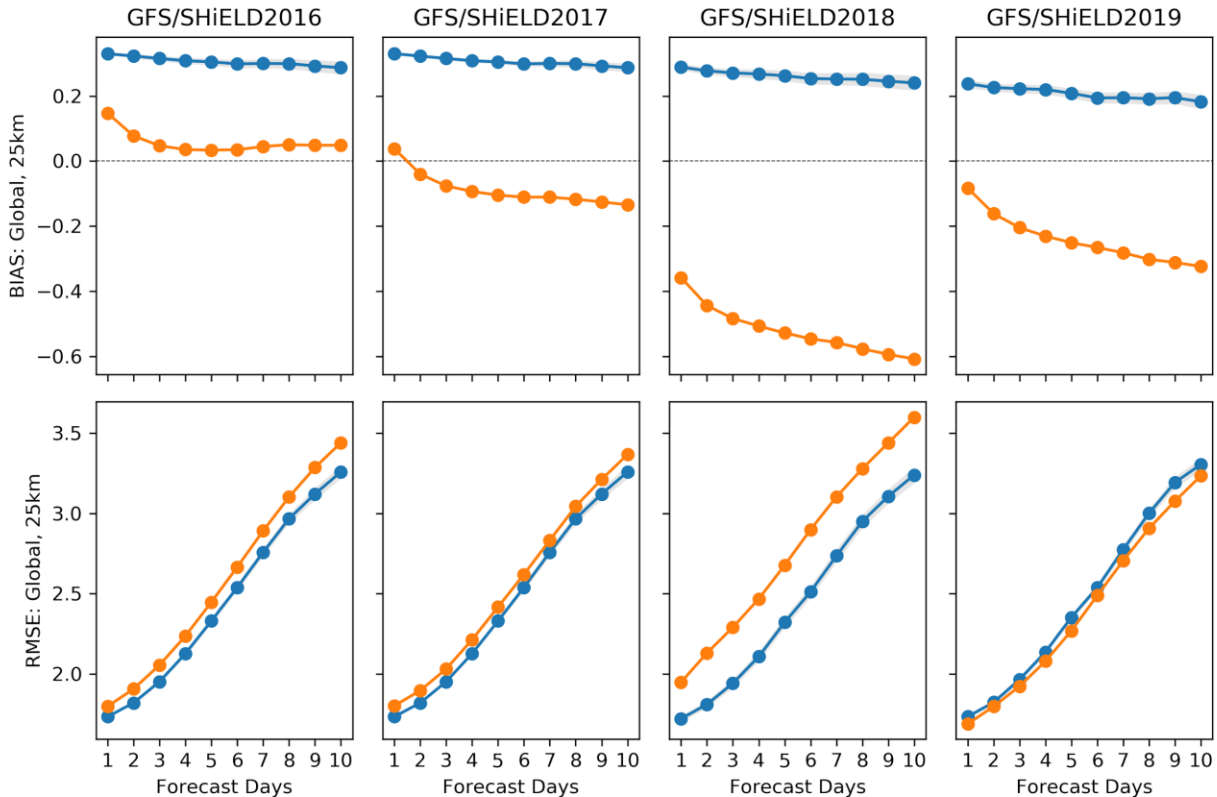
355 **Figure 6.** As in Figure 5 but for precipitation bias, given as bias score minus 1. Here, negative
 356 values imply a low bias.



357

358 **Figure 7.** Precipitation PDF for 13-km SHIELD (orange) compared to contemporary GFS (blue).
 359 Top: Tropical (30S--30N) precipitation vs. TRMM (black). Bottom: CONUS precipitation vs.
 360 StageIV (black).

361 Another sensible weather metric is 2-m temperature, which has an interesting
 362 development history (Figure 8). The initial 2016 version of SHIELD had a very small warm bias,
 363 significantly less than the small (0.3 K) warm bias of the operational GFS. The 2018 version of
 364 SHIELD, which otherwise had significant improvements in other skill metrics, developed a cool
 365 bias which increased to 0.6 K by day 10. Investigation traced the cool bias to two sources: the
 366 switch from the hybrid EDMF PBL to YSU, which by default has significantly less near-surface
 367 mixing and thereby allows the surface to cool too much, and the change in how cloud droplets
 368 absorb radiation when the Inline GFDL Microphysics was introduced. In 2019 the cloud-
 369 radiation interactions were significantly revised, and the background diffusion in the YSU PBL
 370 was increased, which significantly reduced both the cold bias and the error in 2-m temperature.
 371 The cold bias in SHIELD 2019 ranges from 0.1 K on the first day to 0.35 K on day 10, which is
 372 approximately equal to the positive bias of the operational GFS.



373

374 **Figure 8.** Global 2-m temperature (deg K) bias (top) and RMSE (bottom) for 13-km SHiELD
 375 (orange) compared to contemporary GFS (blue), both validated against ERA5 Reanalysis (C3S,
 376 2017).

377

2.2 T-SHiELD North Atlantic Nest for Tropical Cyclone Prediction

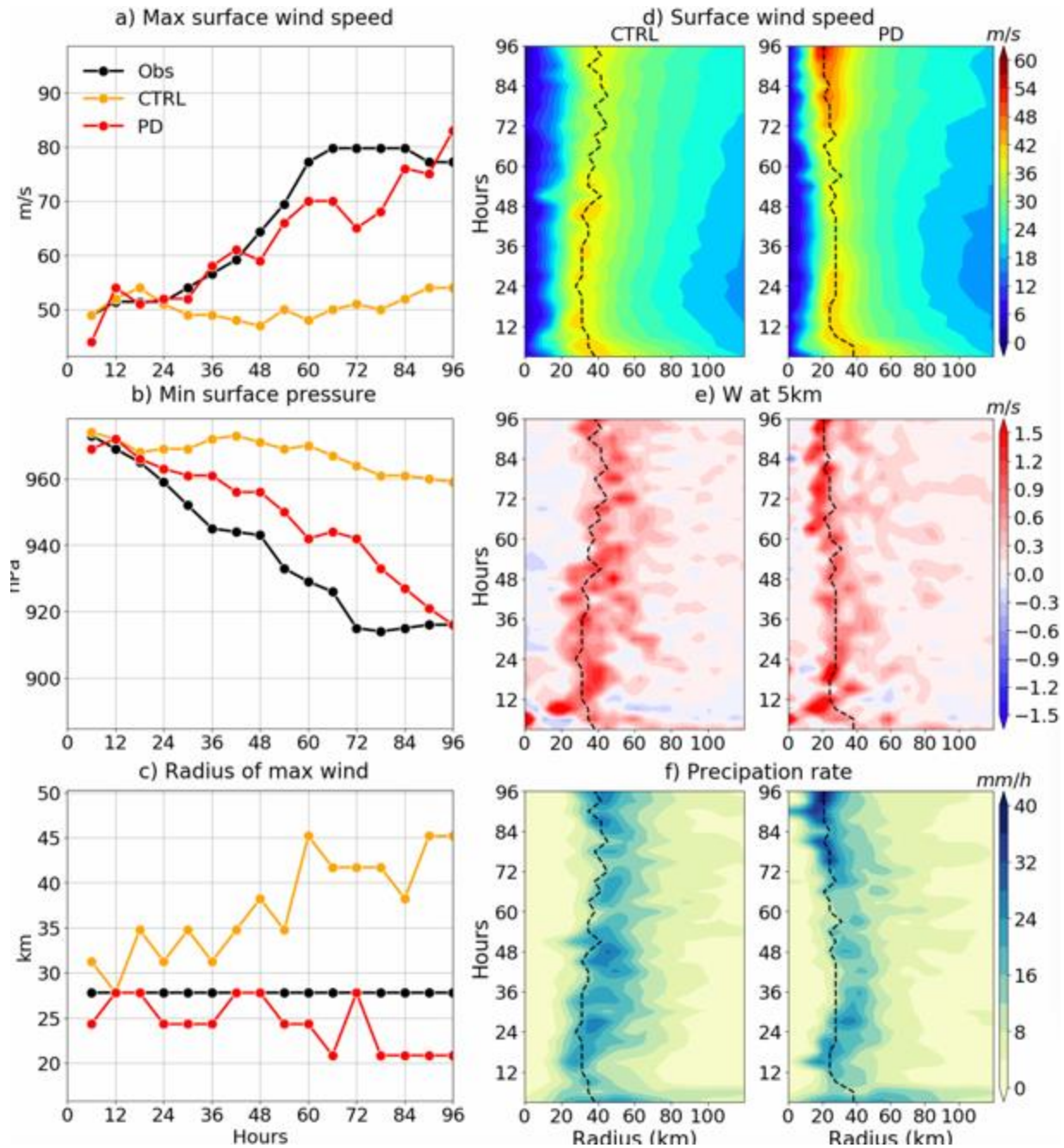
378

379 T-SHiELD uses the variable-resolution capabilities of FV3 to replicate the tropical
 380 cyclone track skill of global models and the intensity skill of convective-scale regional hurricane
 381 models. This configuration uses the 13-km SHiELD grid and then places a large factor-of-four
 382 two-way nest over the tropical North Atlantic (Figure 1). The resulting nested domain has grid
 383 cells of about 3-km width and interacts with its parent global domain. Earlier experiments and a
 384 comprehensive evaluation of T-SHiELD 2017 were described in Hazelton et al. (2018a, 2018b).
 385 T-SHiELD has been used as the initial prototype for the Hurricane Analysis and Forecast System
 386 (HAFS; Hazelton et al., 2020). Here we will describe further evolution of T-SHiELD, including
 387 progress towards rectifying two forecast issues in T-SHiELD 2017: an under-intensification bias
 388 for rapidly intensifying storms, and storms with a radius of maximum winds (RMW) that is too
 large. Note that there is no 2019 version of T-SHiELD.

389

390 Hazelton et al. (2018b) found that the RMW in T-SHiELD 2017 was often larger than
 391 observed and in particular larger than that in HWRF simulations from the same set of cases
 392 Zhang et al. (2015) found that reducing the parameterized mixing in the PBL scheme reduced the
 393 size of the RMW in HWRF. While reducing the parameterized mixing in the hybrid EDMF
 394 scheme gave modest improvement to hurricane structure in T-SHiELD, there was no appreciable
 reduction in the size of the eyewall. A dramatic and immediate impact was instead found by

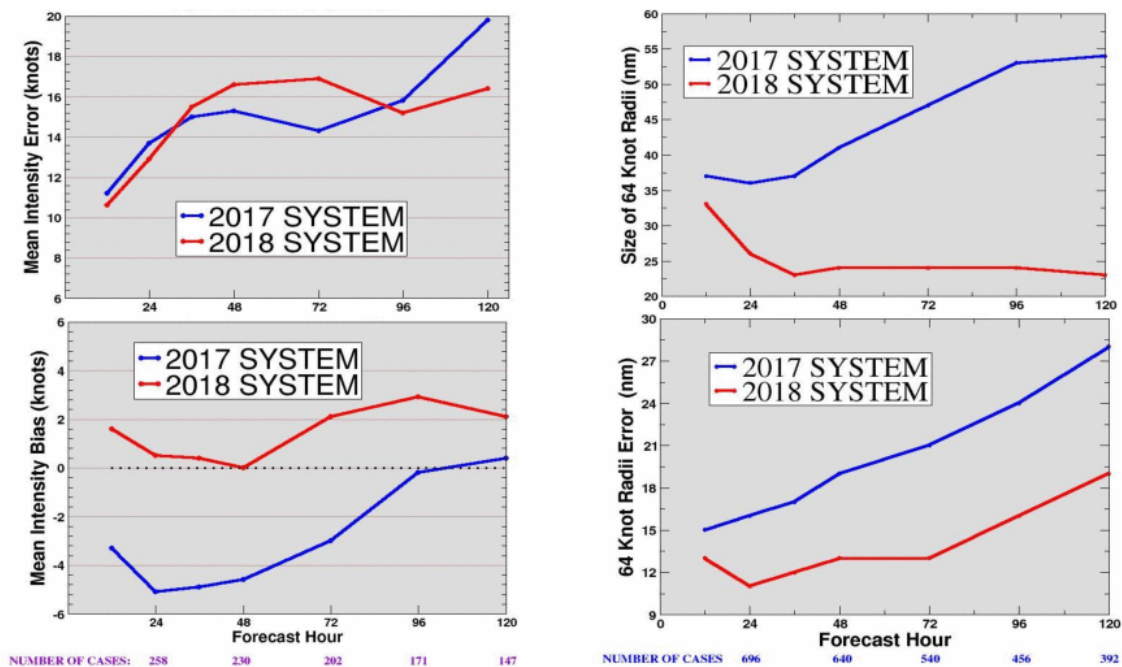
395 using the positive-definite (PD) advection scheme for water vapor and microphysical tracers.
396 Results from T-SHiELD 2018 simulations of Major Hurricane Irma, initialized prior to its rapid
397 intensification, show that a simulation using the older monotonic advection scheme (Figure 9)
398 produces a gradually expanding vortex that does not intensify. Meanwhile, the simulation with
399 the new PD scheme and *no other changes to the physics or dynamics, including advection of*
400 *dynamical quantities*, produces an intensifying storm with a contracting eyewall. Notably, the
401 vertical velocity within the eyewall is much more coherent with the PD scheme and is
402 continually displaced within the eyewall, which we suspect may be driving both the
403 intensification of Irma and a continued contraction of the eye, as well as contributing to
404 enhanced precipitation within the eyewall. For this reason, the positive-definite advection
405 scheme was selected for T-SHiELD 2018.



406

407 **Figure 9.** Hurricane Irma (2017) forecast initialized at 00 UTC 03 September 2017. Left column
 408 shows time-series plots of maximum 10-m winds (a), minimum central pressure (b), and RMW
 409 (c) compared against extended Best Track observations (Demuth et al. 2006). Right column
 410 shows time-radius plots of azimuthally averaged (d) 10-m winds (e) 5-km vertical velocity and
 411 (f) precipitation rate from forecasts of Hurricane Irma initialized 03 September 2017, from a
 412 prototype of T-SHiELD 2018 with the monotonic (CTRL) and positive-definite tracer advection
 413 schemes (PD). The RMW is denoted as a dashed black line. Note that a localized extremum (left
 414 panels) may not be visible in the azimuthal averages (right panel), especially during rapid
 415 intensification.

416 A more systematic comparison of wind radii between the 2017 and 2018 T-SHiELD
 417 versions (Figure 10, right) shows that the effect of the PD scheme is not limited to a single storm.
 418 Noting that the difference between the two T-SHiELD versions is greater than just the PD
 419 scheme, we do see a systematic and substantial decrease in the radius of the 64-kt (33 m s^{-1} ,
 420 hurricane force) winds in the 2018 version. The 2018 version spins up the vortex such that within
 421 36 hours of initialization, the 64-kt radii reduce to and then remain a consistent 20–25 nautical
 422 miles (37–46 km) for the rest of the forecast period. This represents a reduction of more than half
 423 at 120-h lead time compared to the 2017 version, which steadily widens the 64-kt radii during
 424 the simulation. There is also a reduction in radii forecast errors compared to Best Track estimates
 425 in T-SHiELD 2018, with the qualification that there is considerable (potentially 40% for 64-kt:
 426 Landsea and Franklin 2013) uncertainty in estimates of wind radii. This uncertainty can impact
 427 the initialization of tropical cyclones using real-time storm message files (Bender et al. 2017),
 428 and thereby of estimates of size-related impacts like precipitation and extreme winds.



429

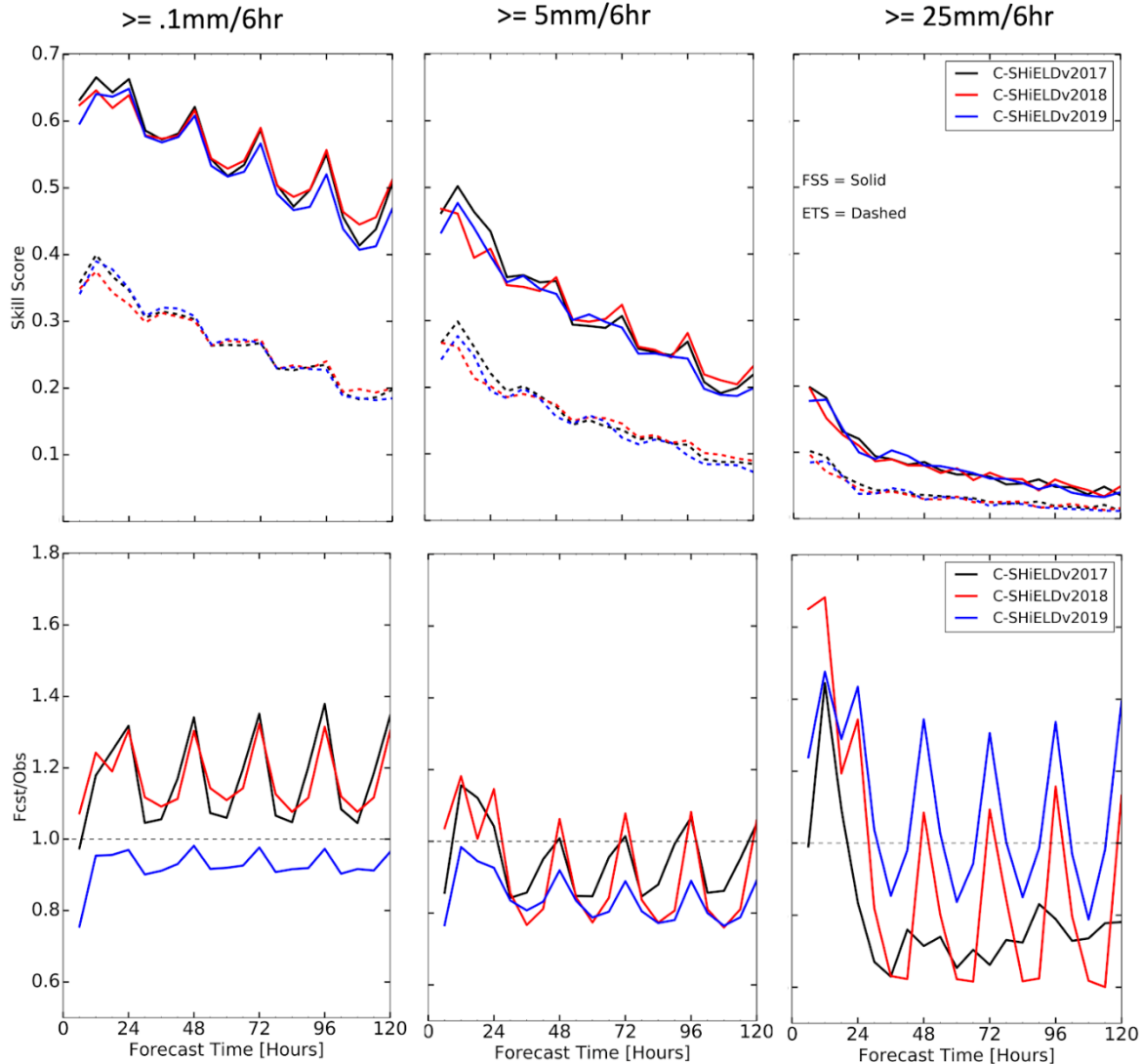
430 **Figure 10.** Verification of intensity (left) and 64-kt radii (33 m s^{-1} , hurricane-force; right)
 431 forecasts for the 2017 and 2018 versions of T-SHiELD during the 2017 Atlantic hurricane season
 432 compared to the Best Track dataset. Units shown (kt, nautical miles) are standard for US
 433 operational prediction.

434 The multiple changes in the 2018 version of T-SHiELD combined to create tropical
 435 cyclones which are stronger overall (Figure 10, left), with little to no bias towards more intense
 436 storms at all lead times. The adoption of the PD scheme and YSU PBL scheme likely created
 437 forecasts of more intense storms mitigated by the introduction of the interactive mixed-layer
 438 ocean. While the weak bias of the 2017 version was alleviated, intensity predictions were not
 439 appreciably improved except at 120-h lead time, and in fact were degraded between 36 and 72
 440 hours after initialization. These results show once again the great challenge of improving
 441 intensity prediction. The reduction in RMWs in simulations using the PD scheme will be
 442 discussed in more detail in a forthcoming manuscript.

443 2.3 C-SHiELD Nest for Continental US Convection

444 C-SHiELD was designed to efficiently reach convective-scale resolutions in a global
445 domain, in this case to replicate the capability of regional convective-scale models for
446 continental convection such as the 3-km NAM Nest and the members of the [High-Resolution
447 Ensemble Forecast \(HREF\)](#). C-SHiELD also is designed to extend convective-scale forecasts
448 beyond the 18-to 60-hour ranges of existing US operational CONUS models into the medium-
449 range timescales and beyond. The nested domain of C-SHiELD serves as a prototype for the
450 Regional Forecast System (RFS; Carley et al. 2020) and the Rapid-Refresh Forecast System
451 (RRFS; Alexander et al. 2020), both using the regional domain capability being developed
452 within FV3 (T. Black, personal communication).

453 The 2017 version of C-SHiELD is described in Harris et al. (2019). Modified versions of
454 C-SHiELD with different microphysics and PBL schemes are described in Zhang et al. (2018)
455 and Snook et al. (2019). C-SHiELD 2018 saw considerable updates as shown in Table 2; C-
456 SHiELD 2019 added incremental updates, including re-configuration of the numerical diffusion
457 and GFDL microphysics. We will limit our discussion to the evolution of broad forecast
458 characteristics, but we will perform year-round validation instead of restricting the analysis to a
459 single season. The exception is for the Surrogate Severe verification below, which is only
460 verified for peak severe weather season of April to August.



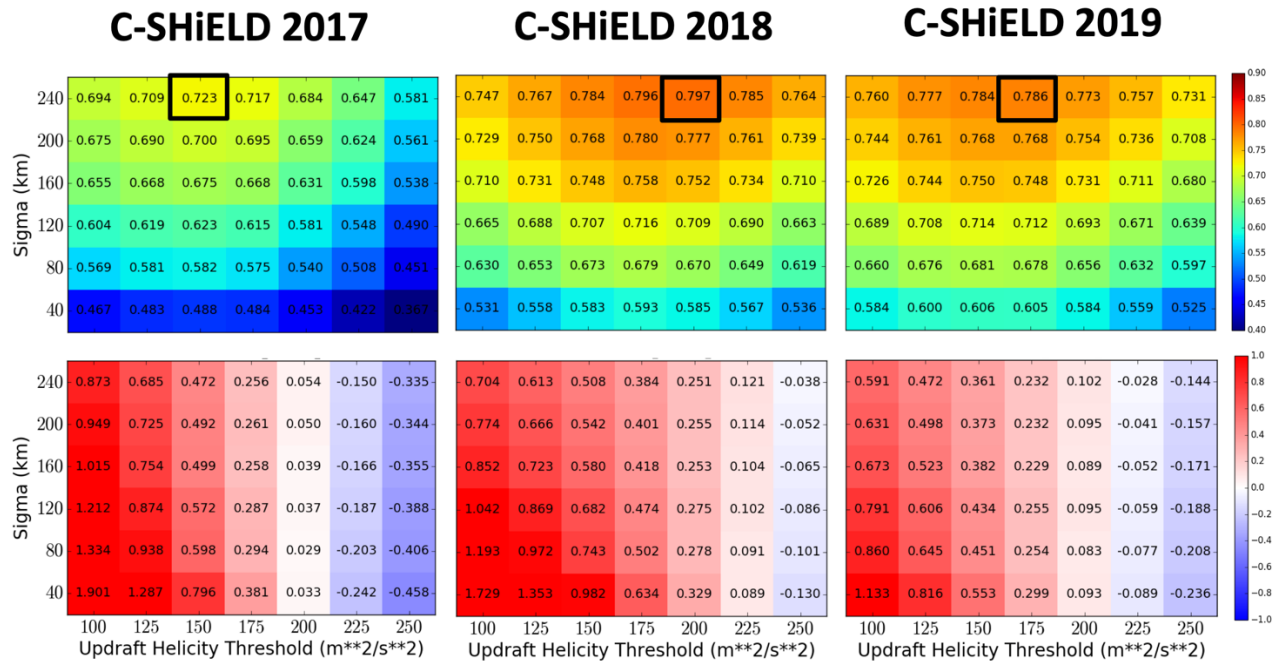
461
 462 **Figure 11.** Precipitation skill scores (top) and bias score (bottom) vs. StageIV for 6-hr CONUS
 463 precipitation in three versions of C-SHIELD, given for precipitation events greater than three six-
 464 hourly accumulation thresholds (0.1, 5.0, and 25.0 mm). Skill scores are given for both Equitable
 465 Threat Score (ETS; Hogan and Mason 2012) and Fractions Skill Score (FSS; Roberts and Lean
 466 2008). C-SHIELD 2017 is validated from May 2017 to May 2018; C-SHIELD 2018 is validated
 467 from April 2018 to May 2019; C-SHIELD 2019 is validated from January to December 2019.
 468 Validation is performed on the 4-km StageIV grid using 3x3 neighborhoods, corresponding to a
 469 12-km radius.

470 Precipitation forecast skill (Figure 11, top panels) is similar among all three versions of
 471 C-SHIELD. The 2019 version has the least overall bias (Figure 11, bottom panels) as earlier
 472 versions had too much light and too little heavy precipitation. The 2019 version reduced the
 473 diurnal cycle in the bias of light and moderate precipitation, although this was still apparent in
 474 the bias score for heavy precipitation and still had a prominent high bias of heavy precipitation
 475 during the first 30 hours. We speculate that the re-configuration of the numerical diffusion,
 476 which improved storm placement, and the revised settings for the GFDL microphysics, which

477 improved structure and evolution of the storms, combined to improve the biases in the 2019
478 version.

479 We use the surrogate severe technique of Sobash et al. (2011) to validate our 2–5 km
480 updraft helicity (UH) fields against storm reports from the Storm Prediction Center. We create
481 surrogate severe fields and validate against observed severe fields to compute FSS and Bias
482 scores in C-SHiELD and plot the results as a function of UH threshold and smoothing radius
483 (Figure 12), similar to Figure 17 in Sobash et al. (2016). For all versions of C-SHiELD the
484 highest FSS is found from the largest smoothing radius of 240 km and for UH thresholds of 150–
485 200 $\text{m}^2 \text{s}^{-2}$, with slightly higher or lower thresholds giving similar skill scores. The UH threshold
486 giving the best score for C-SHiELD is higher than in many other convective-scale models due to
487 the significantly higher updraft helicities in FV3-based models (Potvin et al. 2019). This in turn
488 is likely due to the emphasis on vorticity in the horizontal discretization as described in
489 Harris2019.

490 The maximum FSS in the 2018 and 2019 versions is about 0.8, on par with operational
491 and research convective-scale models (cf. Sobash et al. 2019) and significantly higher than the
492 2017 version. There is a uniform over-prediction bias for all but the highest UH thresholds
493 (Figure 12, bottom row). This bias was significant in the 2017 version but is decreased every
494 year for most threshold-radius combinations, and for the highest-FSS combination decreases
495 from 0.47 in 2017 to 0.22 in 2019. C-SHiELD 2019 still has a high frequency bias except for the
496 very highest UH thresholds, as it is still too aggressive at creating strong storms.



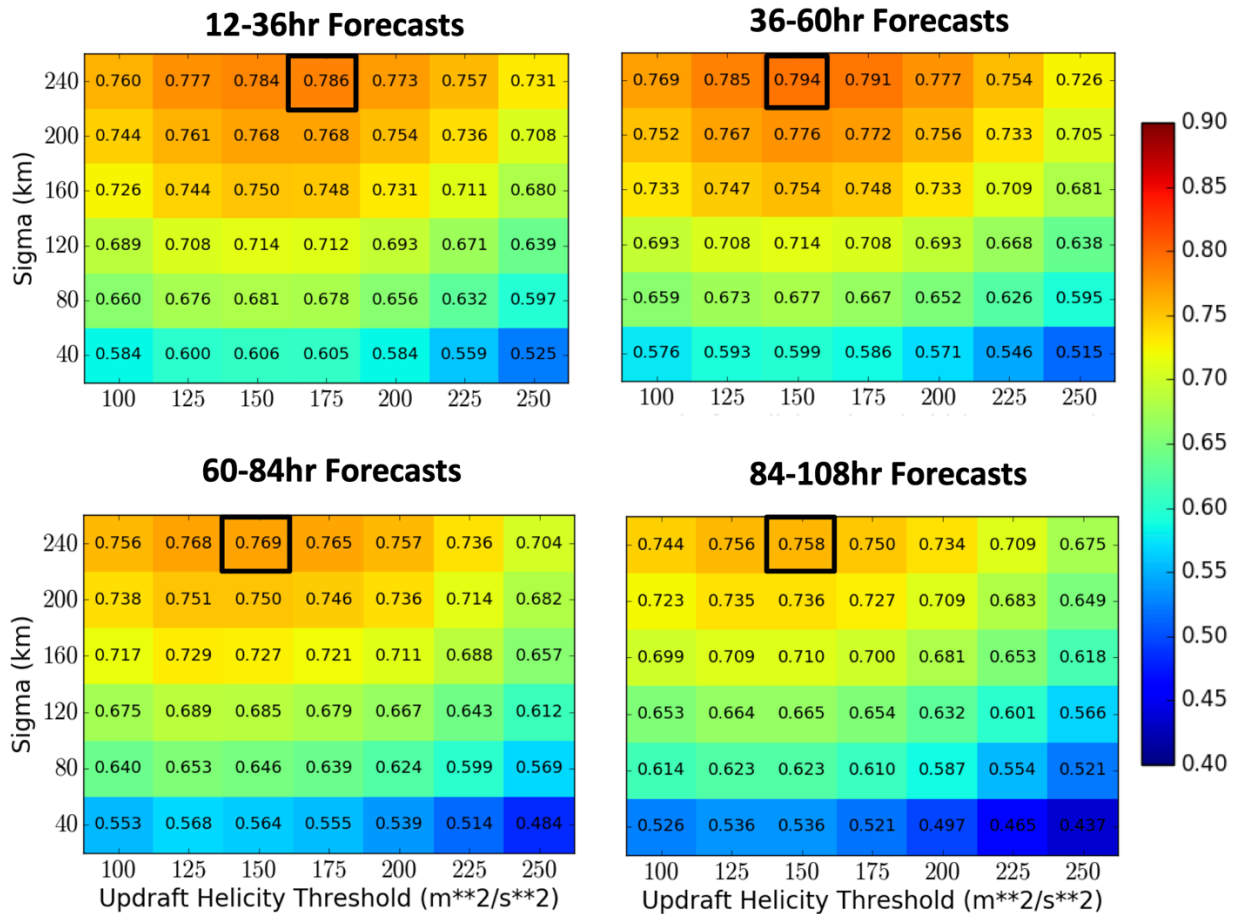
497

498 **Figure 12.** FSS (top) and Bias score minus 1 (bottom) for surrogate severe predictions with 12–
 499 36 hour lead times for three versions of C-SHiELD initialized at 00Z. Heavy black outline
 500 corresponds to the combination of UH threshold (m^2s^{-2}) and smoothing radius (sigma, km)
 501 giving the highest FSS.

502 We also investigate if skillful prediction of severe weather is possible beyond the first
 503 forecast day. Figure 13 shows surrogate severe FSS for days 1 through 4 (hours 12–36, 36–60,
 504 60–84, and 84–108, respectively). The FSS value is not as high on later days as on the first, but
 505 even on day 4 the FSS is still a respectable 0.74, indicating that there is skill in predicting severe
 506 weather multiple days in advance. These high skill scores may be partially due to the relatively
 507 large smoothing radius of 240 km.

508 These multiple-day severe weather forecasts are in the spirit of the convective outlooks
 509 issued by the Storm Prediction Center (www.spc.noaa.gov/products/outlook; Edwards 2015)
 510 based on predictions of synoptic-scale environments favorable for severe weather. The advantage
 511 of using a dynamical convective-scale prediction model on medium-range timescales is that
 512 explicit prediction of storms, instead of just environments, potentially can give forecasts of
 513 convective modes and specific hazards.

514 **Figure 13.** FSS for surrogate severe predictions at different lead times for 00Z



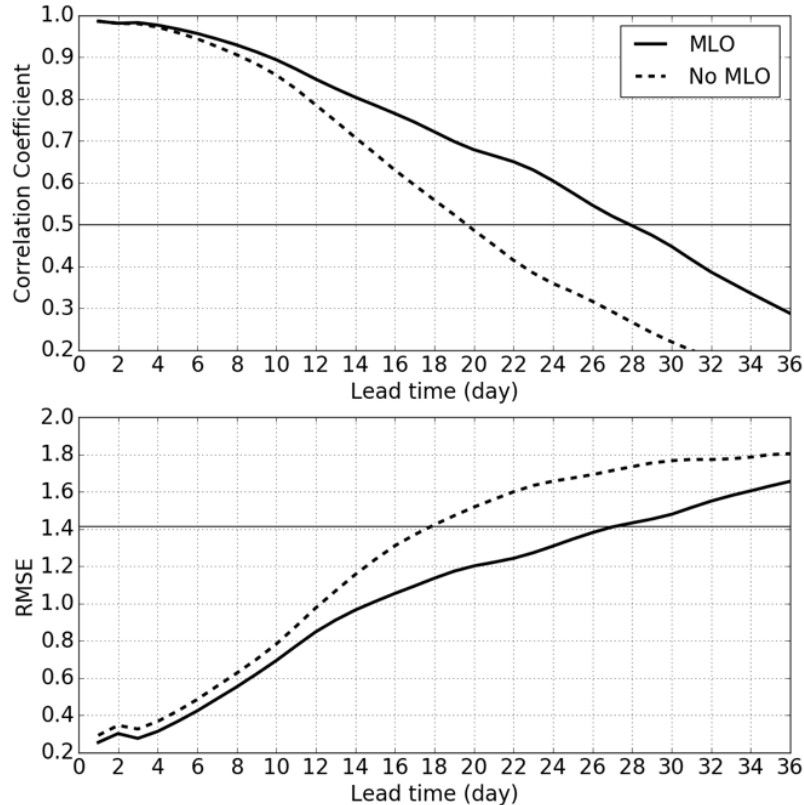
515 initializations of C-SHiELD 2019.

516 2.4 S-SHiELD Subseasonal-to-Seasonal Prediction

517 We briefly describe the characteristics of the Tier-2 S-SHiELD configuration, using a 25-
 518 km grid designed for climate integrations and for subseasonal and seasonal predictions. S-
 519 SHiELD is configured similarly to the 13-km SHiELD, although SHiELD's two-day relaxation
 520 timescale of SSTs in the MLO towards the "frozen anomalies" is extended to 15 days in S-
 521 SHiELD.

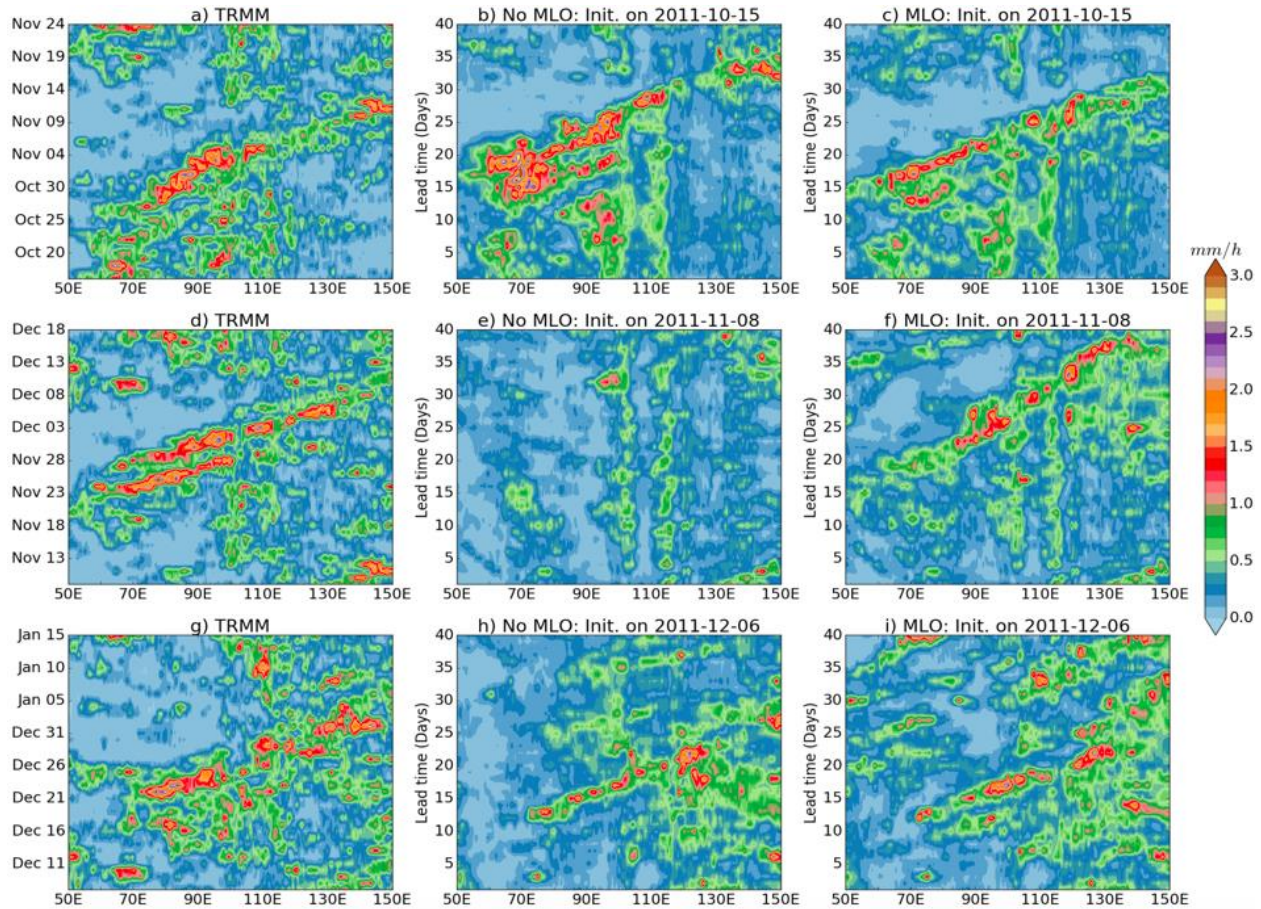
522 The MJO plays a major role in subseasonal variability but has been a challenge for many
 523 models to predict or even simulate reasonably (Kim et al. 2018). To explore the MJO prediction
 524 skill of S-SHiELD we performed 92 40-day predictions, one initialized at 00Z every two days
 525 from 1 October 2011 to 31 March 2012, covering the active Dynamics of the MJO (DYNAMO;
 526 Yoneyama et al. 2013) observation period. The Real-time Multivariate MJO Index (RMM;

527 Wheeler and Hendon 2004) is calculated following the methodology of Xiang et al. (2015) and
 528 Vitart et al (2017). We find that S-SHiELD with the MLO (Figure 14) has good skill (correlation
 529 > 0.7) out to 19 days and useful skill (correlation > 0.5) out to 28 days. The RMSE likewise
 530 shows similar skill ($\text{RMSE} < \sqrt{2}$ out to 27 days).



531
 532 **Figure 14.** Prediction skill of the MJO's RMM indices in S-SHiELD with (solid) and without
 533 (dotted) the interactive MLO for 92 40-day predictions initialized during the 2011-2012
 534 DYNAMO period. Top: Correlation coefficient; bottom: RMSE.

535 The behavior of the MJO in GFDL's CMIP6-generation climate models (Zhao et al.
 536 2018) suggests that the two keys for a good MJO simulation are an appropriate convection
 537 scheme and some form of interactive ocean, which has also been found by DeMott et al. (2019)
 538 and others. A second set of S-SHiELD experiments was performed using climatological SSTs
 539 plus frozen anomalies. These simulations without the interactive MLO had much smaller RMM
 540 correlations, with predictions no longer useful after day 20, and larger errors. The effect of the
 541 interactive ocean is made clear in Figure 15, in which S-SHiELD with the MLO correctly
 542 predicted the formation of all three strong MJO events during this period 10–15 days in advance,
 543 and correctly propagated all events through the Maritime Continent (near 120 E longitude),
 544 although the propagation speed is slower than observed and there is some disruption near the
 545 Maritime Continent. However, S-SHiELD with prescribed SSTs has difficulty propagating the
 546 MJO through the Maritime Continent and for the November event creates no MJO whatsoever.
 547 The November event proves particularly challenging for S-SHiELD without the MLO as it
 548 performs poorly at a range of lead times (Supplemental Figure S2) but poses no problem for S-
 549 SHiELD with the MLO. It is clear that the simple, inexpensive MLO used in S-SHiELD is
 550 sufficient to significantly extend the predictability of the MJO.

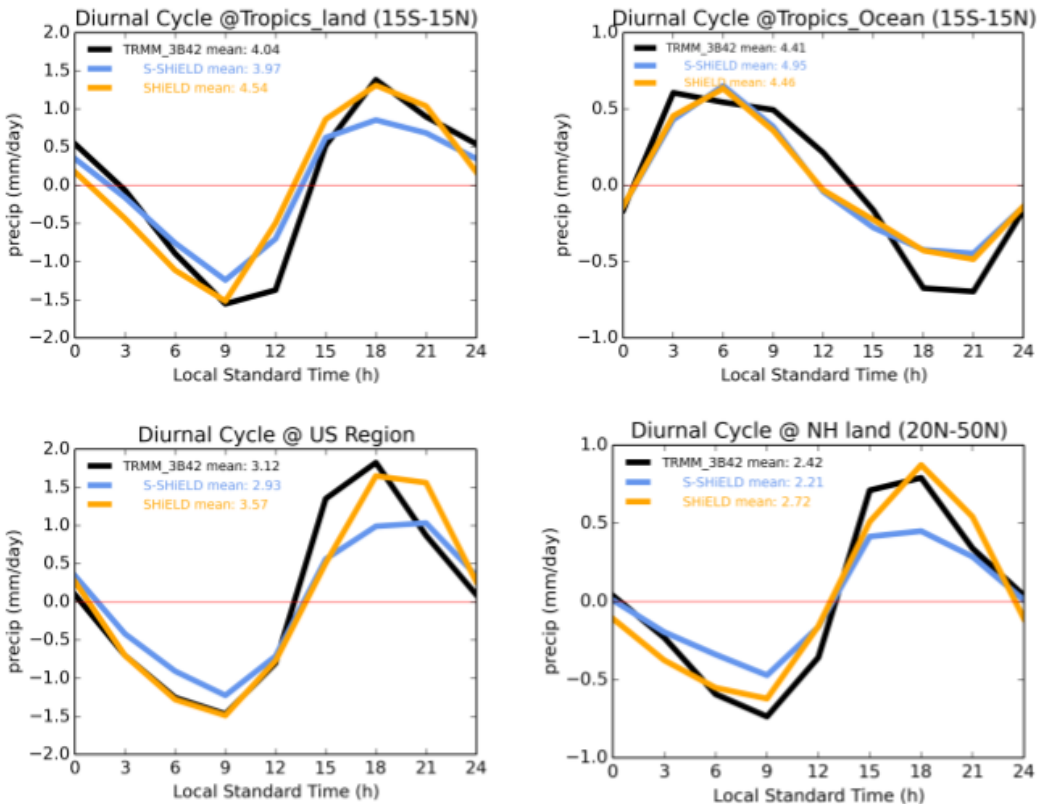


551
 552 **Figure 15.** Precipitation (averaged from 5S--5N) from TRMM (left), S-SHiELD without MLO
 553 (center), and S-SHiELD with MLO (right), for initializations at (top) 15 October (middle) 8
 554 November and (bottom) 6 December 2011.

555 Klingaman and DeMott (2020) found that climate models exaggerate the effect of ocean
 556 coupling on the MJO by over-intensifying the MJO in El Niño years. S-SHiELD does not have a
 557 coupled dynamical ocean and nudges towards climatology, and so can only represent the El
 558 Niño-Southern Oscillation (ENSO) state at initialization; indeed, the DYNAMO period was
 559 during a La Niña event (see
 560 https://origin.cpc.ncep.noaa.gov/products/analysis_monitoring/ensostuff/ONI_v5.php). Hence,
 561 this ENSO contamination of the link between ocean coupling and the MJO is not present in S-
 562 SHiELD.

563 The diurnal cycle of precipitation is another challenge for climate models. Covey et al
 564 (2016) found nearly all climate models, even the 30-km resolution GFDL HiRAM, struggle with
 565 both the phase and amplitude of the diurnal cycle, especially over land and during boreal
 566 summer. Figure 16 presents the JJA diurnal cycle from a 10-year S-SHiELD simulation with
 567 MLO SSTs nudged towards climatology, with results from 13-km SHiELD hindcasts shown for
 568 reference. We find that the observed phase of the diurnal cycle is beautifully matched by S-
 569 SHiELD, over both land and ocean. Most notably the CONUS evening maximum of
 570 precipitation is reproduced. However, the amplitude of the cycle is biased low over land areas,
 571 possibly due to the inability of S-SHiELD's 25-km grid to produce the propagating mesoscale
 572 convective systems characteristic of heavier warm-season precipitation. This appears to

573 be a resolution effect as 13-km SHiELD reproduces both the correct phase and amplitude of
 574 precipitation. We also find that the majority of precipitation in S-SHiELD (55% globally and
 575 80% between 20S and 20N) is from the SAS convective scheme, although this does not
 576 adversely affect the phase of the diurnal cycle. S-SHiELD does have the correct phase and
 577 amplitude (albeit slightly too high) of the diurnal cycle of 2-m temperature over land
 578 (Supplemental Figure S3).



579 **Figure 16.** JJA diurnal cycle of precipitation as a function of local solar time in a 10-year S-
 580 SHiELD climate integration with the MLO nudged towards climatological SSTs, and from days
 581 6--10 of three years of 13-km SHiELD hindcasts (initialized every five days), compared to
 582 TRMM 2011-2018 observations. Means are given in the legends as mm/day.
 583

584 Hagos et al. (2016) found that the diurnal cycle of cloudiness and precipitation plays a
 585 key role in the propagation of the MJO through the Maritime Continent. Since S-SHiELD has
 586 considerably better diurnal cycles of precipitation and temperature over land, especially over
 587 tropical land, than do most climate models, we might expect that this improved representation of
 588 the diurnal cycle may be contributing to the improved representation of the MJO seen above.

589 4 Conclusion and Prospects

590 We have developed the SHiELD modeling system as a research tool to demonstrate new
 591 capabilities of the FV3 Dynamical Core and of our physical parameterizations, develop new
 592 ideas in atmospheric prediction modeling, and to explore processes and phenomena within the
 593 atmosphere. Since late 2015 when FV3 was first coupled to the then-operational GFS Physics

594 Driver we have developed SHiELD into a promising vehicle for improving the prediction and
595 understanding of atmospheric phenomena. SHiELD also demonstrates the potential and viability
596 of unified modeling in which there is a single modeling system with one codebase, one
597 executable, one preprocessor, one set of runscripts, and one set of post-processing tools. This
598 greatly simplifies the modeling suite and allows improvements to be exchanged between
599 configurations.

600 The fundamental characteristics of SHiELD compared to previous-generation and
601 existing operational models are documented in this and other publications. For some applications
602 we have previously demonstrated capabilities similar to that of existing modeling systems, such
603 as severe-storm prediction in C-SHiELD (Harris et al 2019) and tropical cyclone intensity
604 prediction in T-SHiELD (Hazelton et al 2018a,b). We have shown significant improvements
605 over existing models, especially over existing global models, for large-scale and hurricane
606 prediction skill in 13-km SHiELD (Zhou et al 2019, Chen et al 2019a), and the diurnal cycle and
607 MJO prediction in S-SHiELD. We have even shown entirely new possibilities for prediction
608 modeling, such as skillful hurricane intensity forecasts in 13-km SHiELD (Chen et al. 2019b),
609 and the possibility of medium-range convective-scale prediction in C-SHiELD. *Ultimately, the*
610 *true strength of SHiELD is that all of these characteristics are demonstrated in the same*
611 *modeling system.*

612 SHiELD is designed to be an experimental research modeling system, with a particular
613 set of scientific goals set by its developers, and thereby is more restricted in scope than the GFS,
614 HAFS, RFS, and other general-purpose models intended for operational weather forecasting and
615 to support broad audiences of users. While improved prediction skill is a major scientific goal
616 and an important “vital sign” of model development, we also develop SHiELD as a means to
617 demonstrate new modeling capabilities. SHiELD is also intended to be principally a physical
618 atmosphere modeling system and is not intended for research into oceanic dynamics, decadal-to-
619 centennial projection, biogeochemistry, or other topics taking place at either longer timescales or
620 greater complexity than SHiELD is designed for. Improvements within SHiELD can be
621 seamlessly transitioned into other FV3-based models that do address these topics, including other
622 Unified Forecast System models and the FV3-based coupled earth-system models at GFDL,
623 within NASA, NCAR, and elsewhere. As such SHiELD’s progress will continue to contribute to
624 the development and improvement of these modeling systems. SHiELD is a part of GFDL’s
625 fourth-generation modeling suite (GFDL 2019, Figures 1 and 2) and shares common
626 infrastructure with CM4, ESM4, and SPEAR. SHiELD uses a different physics suite and land
627 model from the other GFDL configurations, but otherwise is constructed similarly. Advances can
628 then be exchanged between the configurations, allowing for mutual improvement, seamless
629 cross-timescale modeling, and potentially unification of GFDL’s weather and climate modeling
630 efforts.

631 Further development of SHiELD, including both FV3 and the SHiELD physics, will
632 continue to improve the prediction skill of the configurations, address issues which have been
633 identified, and broaden the scope towards new applications. As computing power allows, models
634 will be pushed to higher horizontal and vertical resolution, physical processes developed to
635 improve simulation quality and prediction skill, and to address emerging scientific questions.
636 New capabilities within FV3, including regional and doubly periodic domains, will permit
637 efficient simulation of processes at kilometer and sub-kilometer scales for basic science and for
638 process studies to improve physical parameterizations. We are also working on a native SHiELD

639 data assimilation cycling system to take advantage of the new advances and to create initial
 640 conditions most consistent with the forward prediction model configurations. Finally,
 641 development will continue of our Tier-2 configurations, with near real-time S2S predictions
 642 being made using S-SHiELD, and continued extension into the global cloud-resolving regime
 643 (cf. Stevens2019) towards new scientific problems not adequately addressed by existing regional
 644 models or by coarse-resolution global models.

645 **Acknowledgments**

646 SHiELD grew out of a major collaboration between GFDL and EMC and would not have been
 647 possible without the physical parameterization suite, software, data, and especially input initial
 648 conditions and baseline forecasts made freely available by EMC and the National Weather
 649 Service. We thank Jongil Han for providing SA-SAS, and George Gayno and Helin Wei for
 650 providing EMC pre-processing tools and land model inputs and for significant assistance with
 651 these tools and datasets. We also thank James Franklin (NHC, retired) for advice on the accuracy
 652 of the wind radii in the best-track dataset. Kate Zhou and Tom Delworth provided reviews of this
 653 manuscript. Xi Chen, Linjiong Zhou, Kun Gao, Yongqiang Sun, Kai-Yuan Cheng, and Morris
 654 Bender are funded under award NA18OAR4320123 from the National Oceanic and Atmospheric
 655 Administration, U.S. Department of Commerce. Xi Chen, Zhou, and Cheng were additionally
 656 funded by the Next-Generation Global Prediction System project of the National Weather
 657 Service. Supporting data can be found at <ftp.gfdl.noaa.gov/pub/Lucas.Harris/JAMES-SHiELD/>.

658 **Appendix A: Positive-Definite Advection Scheme**

659 The Lagrangian dynamics in FV3 uses 1D advection operators to build the 2D advection
 660 scheme of Lin and Rood (1996). In hydrostatic FV3 these operators are typically monotonic (Lin
 661 2004), in that no new extrema are created by the advection; however monotonic advection can be
 662 overly diffusive for some applications. In nonhydrostatic FV3 the monotonicity constraint is not
 663 used for advection of dynamical quantities (vorticity, heat, air mass), but positivity still needs to
 664 be enforced for scalar tracers. We introduce a positive-definite scheme, which uses a weaker
 665 constraint than monotonicity which only prevents the appearance of negative values.

666 This positivity constraint can be applied to any scheme similar to VanLeer (1974) or
 667 PPM (Collella and Woodward 1984) in which first-guess continuous edge values $\hat{q}_{i+1/2}$ and
 668 $\hat{q}_{i-1/2}$ are interpolated from the cell-averaged values \bar{q}_i where i is a grid index. As with a
 669 standard monotonicity constraint we break the continuity of the sub-grid reconstructions across
 670 grid-cell interfaces, creating left-edge and right-edge values, Q_i^- and Q_i^+ , respectively, as well as
 671 a curvature value B_{oi} for each grid cell, which are then used to compute the flux as in Putman
 672 and Lin (2007), Appendix B.

673 To adjust the edge values to ensure positivity, we use the algorithm below on cell i ,
 674 where notation is as in Lin (2004), Appendix A:

$$675 \quad Q_i^- = \hat{q}_{i-1/2} - \bar{q}_i$$

$$676 \quad Q_i^+ = \hat{q}_{i+1/2} - \bar{q}_i$$

$$677 \quad B_{oi} = Q_i^- + Q_i^+$$

$$678 \quad \Delta A_i = Q_i^+ - Q_i^-$$

$$\begin{aligned}
679 \quad & A_{4i} = -3 B_{oi} \\
680 \quad & \text{If } \text{abs}(\hat{q}_{i+1/2} - \hat{q}_{i-1/2}) > -A_{4i} \text{ and } \bar{q}_i + \Delta A_i^2 / (4A_{4i}) + \frac{1}{12} A_{4i} < 0 \text{ then} \\
681 \quad & \quad \text{If } Q_i^- Q_i^+ > 0 \text{ then} \\
682 \quad & \quad \quad Q_i^- = Q_i^+ = B_{oi} = 0 \\
683 \quad & \quad \text{Elseif } dA_i > 0 \text{ then} \\
684 \quad & \quad \quad Q_i^+ = -2 * Q_i^- \\
685 \quad & \quad \quad B_{oi} = -Q_i^- \\
686 \quad & \quad \text{Else} \\
687 \quad & \quad \quad Q_i^- = -2 * Q_i^+ \\
688 \quad & \quad \quad B_{oi} = -Q_i^+
\end{aligned}$$

689 **Appendix B: Split and In-line GFDL Microphysics**

690 The GFDL microphysics, a single-moment six-category microphysics, has its origin in
691 the microphysics of Lin et al. (1983) as implemented within GFDL ZETAC (Pauluis and Garner,
692 2006; Knutson et al., 2007, 2008) with further developments from Lord et al. (1984) and Krueger
693 et al. (1995). It was later substantially revised for use in HiRAM (Chen and Lin, 2011, 2013;
694 Harris et al., 2016; Gao et al., 2017, 2019) by adding the following updates:

- 695 1. Time-splitting is applied between warm-rain and ice-phase processes, with the warm-rain
696 processes called twice per invocation.
- 697 2. PPM is applied for sedimentation of all condensate species except cloud water, ensuring
698 shape preservation and stability.
- 699 3. The heat content of condensates is included when heating/cooling grid cells.
- 700 4. Scale awareness is achieved by assuming a horizontal subgrid distribution and a second-
701 order vertical reconstruction for autoconversion processes with a slope which increases
702 with grid-cell width.
- 703 5. Additional microphysical processes, including ice nucleation and cloud ice
704 sedimentation, were introduced.

705

706 In the Split GFDL Microphysics first implemented within SHIELD, microphysical
707 processes were divided into fast and (relatively) slow processes, where the fast processes
708 (primarily phase changes and latent heating/cooling) are updated after the vertical remapping in
709 FV3, while the slower processes remain in the physical driver. More recently, the entire GFDL
710 microphysics was Inlined within the dynamical core. The advantages of Inlining are 1) to
711 separate the physical processes based on different time scales to better interact with dynamics
712 processes; and 2) to be able to make the physical parameterization thermodynamically consistent
713 with the dynamical core. Other updates in the Inline microphysics include a time-implicit
714 monotonic scheme for sedimentation to ensure stability without needing to subcycle; precise

715 conservation of the total moist energy; and transportation of heat and momentum carried by
716 condensates during sedimentation.

717 **Appendix C: A Note on Terminology**

718 The term “model” means so many different things in so many contexts that its use can be
719 confusing. In this paper, we use the term “model” only in the abstract (“other general-purpose
720 models”, “NCEP Modeling Suite”) or as part of the name of another system (“Noah Land
721 Surface Model”, “GFDL Hurricane Model”). For concreteness, we refer to SHIELD as a
722 “modeling system” which can be used in a variety of “configurations” (13-km SHIELD, C-
723 SHIELD, T-SHIELD, S-SHIELD), each of is upgraded to new versions yearly (SHIELD 2016,
724 SHIELD 2017, etc.).

725 **References**

- 726 Alexander, C., Carley, J., Heinselman, P. L., & Harris, L. (2020). Advancements of the FV3
727 Stand-Alone Regional Model. In *100th Annual Meeting*. AMS.
- 728 Alpert, J. C. (2004, January). Sub-grid scale mountain blocking at NCEP. In *Proceedings of 20th*
729 *Conference on WAF, 16th conference on NWP*.
- 730 Arnold, N. P., & Putman, W. M. (2018). Nonrotating convective self-aggregation in a limited
731 area AGCM. *Journal of advances in modeling earth systems*, *10*(4), 1029-1046.
- 732 Balaji, V. (2012). The flexible modeling system. In *Earth System Modelling-Volume 3* (pp. 33-
733 41). Springer, Berlin, Heidelberg.
- 734 Bender, M.A., T.P. Marchok, C.R. Sampson, J.A. Knaff, and M.J. Morin. (2017). Impact of
735 Storm Size on Prediction of Storm Track and Intensity Using the 2016 Operational GFDL
736 Hurricane Model. *Wea. Forecasting*, *32*, 1491–1508. <https://doi.org/10.1175/WAF-D-16-0220.1>
- 737 Bender, M. A., Marchok, T., Tuleya, R. E., Ginis, I., Tallapragada, V., & Lord, S. J. (2019).
738 Hurricane Model Development at GFDL: A Collaborative Success Story from a Historical
739 Perspective. *Bulletin of the American Meteorological Society*, *100*(9), 1725-1736.
- 740 Brown, A., et al. (2012). "Unified Modeling and Prediction of Weather and Climate: A 25-Year
741 Journey." *Bulletin of the American Meteorological Society*, *93*(12): 1865-1877.
- 742 Carley, J. R., et al. (2020). Advances toward an Operational Convection-Allowing Ensemble
743 Prediction System in the Unified Forecast System at NOAA. In *100th Annual Meeting*. AMS.
- 744 Chen, J. H., & Lin, S. J. (2013). Seasonal predictions of tropical cyclones using a 25-km-
745 resolution general circulation model. *Journal of Climate*, *26*(2), 380-398.
- 746 Chen, J. H., & Lin, S. J. (2011). The remarkable predictability of inter-annual variability of
747 Atlantic hurricanes during the past decade. *Geophysical Research Letters*, *38*(11).
- 748 Chen, J. H., Chen, X., Lin, S. J., Magnusson, L., Bender, M., Zhou, L., & Rees, S. (2018).
749 Tropical cyclones in GFDL fvGFS—Impacts of dycore, physics and initial conditions. In *33rd*
750 *Conf. on Hurricane and Tropical Meteorology*.

- 751 Chen, J. H., Lin, S. J., Magnusson, L., Bender, M., Chen, X., Zhou, L., ... & Harris, L. (2019).
 752 Advancements in hurricane prediction with NOAA's next-generation forecast
 753 system. *Geophysical Research Letters*, *46*(8), 4495-4501.
- 754 Chen, J. H., Lin, S. J., Zhou, L., Chen, X., Rees, S., Bender, M., & Morin, M. (2019). Evaluation
 755 of Tropical Cyclone Forecasts in the Next Generation Global Prediction System. *Monthly*
 756 *Weather Review*, *147*(9), 3409-3428.
- 757 Chun, H. and J. Baik. (1994). Weakly Nonlinear Response of a Stably Stratified Atmosphere to
 758 Diabatic Forcing in a Uniform Flow. *J. Atmos. Sci.*, *51*, 3109–
 759 3121, [https://doi.org/10.1175/1520-0469\(1994\)051<3109:WNROAS>2.0.CO;2](https://doi.org/10.1175/1520-0469(1994)051<3109:WNROAS>2.0.CO;2)
- 760 Clough, S., Shephard, M., Mlawer, E., Delamere, J., Iacono, M., Cady-Pereira, K., Boukabara,
 761 S., & Brown, P. (2005). Atmospheric radiative transfer modeling: A summary of the AER
 762 codes. *Journal of Quantitative Spectroscopy and Radiative Transfer*, *91*(2), 233–244.
- 763 Colella, P., & Woodward, P. R. (1984). The piecewise parabolic method (PPM) for gas-
 764 dynamical simulations. *Journal of computational physics*, *54*(1), 174-201.
- 765 Copernicus Climate Change Service (C3S) (2017): ERA5: Fifth generation of ECMWF
 766 atmospheric reanalyses of the global climate. Copernicus Climate Change Service Climate Data
 767 Store (CDS), accessed 14 January 2020. <https://cds.climate.copernicus.eu/cdsapp#!/home>
 768
- 769 Covey, C., P.J. Gleckler, C. Doutriaux, D.N. Williams, A. Dai, J. Fasullo, K. Trenberth, and A.
 770 Berg. (2016). Metrics for the Diurnal Cycle of Precipitation: Toward Routine Benchmarks for
 771 Climate Models. *J. Climate*, *29*, 4461–4471. <https://doi.org/10.1175/JCLI-D-15-0664.1>
- 772 de Boyer Montégut, C., Madec, G., Fischer, A. S., Lazar, A., & Iudicone, D. (2004). Mixed layer
 773 depth over the global ocean: An examination of profile data and a profile-based
 774 climatology. *Journal of Geophysical Research: Oceans*, *109*(C12).
- 775 Delworth, T. L., Cooke, W. F., Adcroft, A., Bushuk, M., Chen, J. H., Dunne, K. A., ... &
 776 Harrison, M. J. (2020). SPEAR—the next generation GFDL modeling system for seasonal to
 777 multidecadal prediction and projection. *Journal of Advances in Modeling Earth Systems*.
- 778 Demaria, E. M. C., Palmer, R. N., and Roundy, J. K. (2016). Regional climate change
 779 projections of streamflow characteristics in the Northeast and Midwest U.S. *Journal of*
 780 *Hydrology: Regional Studies*, *5*, March 2016, 309-323.
 781 <https://doi.org/10.1016/j.ejrh.2015.11.007>.
- 782 DeMott, C. A., Klingaman, N. P., Tseng, W.-L., Burt, M. A., Gao, Y., & Randall, D.A. (2019)
 783 The convection connection: How ocean feedbacks affect tropical mean moisture and MJO
 784 propagation. *Journal of Geophysical Research Atmospheres*, *124*, 11910– 11931.
 785 <https://doi.org/10.1029/2019JD031015>
- 786 Demuth, J. L., DeMaria, M., & Knaff, J. A. (2006). Improvement of advanced microwave
 787 sounding unit tropical cyclone intensity and size estimation algorithms. *Journal of applied*
 788 *meteorology and climatology*, *45*(11), 1573-1581.

- 789 Dong, J., and coauthors. (2020). The Evaluation of Real-Time Hurricane Analysis and Forecast
790 System (HAFS) Stand-Alone Regional (SAR) Model Performance for the 2019 Atlantic
791 Hurricane Season. *Atmosphere*, 11(6), 617. <https://doi.org/10.3390/atmos11060617>
- 792 Dunne, J., and coauthors. (2020). The GFDL Earth System Model version 4.1 (GFDL-ESM4.1):
793 Model description and simulation characteristics. Submitted to *J. Adv. Modeling Earth Sys.*
- 794 Edwards, R. (2015). Overview of the Storm Prediction Center. In *13th History Symposium*.
- 795 ECMWF. (2019). Part III: Dynamics and Numerical Procedures. *IFS Documentation CY46R1*.
- 796 ECMWF. (2019). Part IV: Physical Processes. *IFS Documentation CY46R1*.
- 797 Ek, M. B., Mitchell, K. E., Lin, Y., Rogers, E., Grunmann, P., Koren, V., Gayno, G., & Tarpley,
798 J. D. (2003). Implementation of Noah land surface model advances in the National Centers for
799 Environmental Prediction operational mesoscale Eta model. *Journal of Geophysical*
800 *Research*, 108(D22), 8851. <https://doi.org/10.1029/2002JD003296>
- 801 Gao, K., Chen, J. H., Harris, L. M., Lin, S. J., Xiang, B., & Zhao, M. (2017). Impact of
802 intraseasonal oscillations on the tropical cyclone activity over the Gulf of Mexico and western
803 Caribbean Sea in GFDL HiRAM. *Journal of Geophysical Research: Atmospheres*, 122(24), 13-
804 125.
- 805 Gao, K., Chen, J. H., Harris, L., Sun, Y., & Lin, S. J. (2019). Skillful Prediction of Monthly
806 Major Hurricane Activity in the North Atlantic with Two-way Nesting. *Geophysical Research*
807 *Letters*, 46(15), 9222-9230.
- 808 GFDL. (2019). The 5–10 Year Strategic Plan. Available at [https://www.gfdl.noaa.gov/wp-](https://www.gfdl.noaa.gov/wp-content/uploads/2019/10/2019_GFDL_External_Review_Strategic_Plan.pdf)
809 [content/uploads/2019/10/2019_GFDL_External_Review_Strategic_Plan.pdf](https://www.gfdl.noaa.gov/wp-content/uploads/2019/10/2019_GFDL_External_Review_Strategic_Plan.pdf)
- 810 Haarsma, R., van der Linden, E. C., Selten, F., & van der Schrier, G. (2017). Extreme future
811 central European droughts in a high-resolution global climate model. In *EGU General Assembly*
812 *Conference Abstracts* (Vol. 19, p. 14128).
- 813 Hagos, S. M., Zhang, C., Feng, Z., Burleyson, C. D., De Mott, C., Kerns, B., Benedict, J. J., and
814 Martini, M. N. (2016). The impact of the diurnal cycle on the propagation of Madden-Julian
815 Oscillation convection across the Maritime Continent. *J. Adv. Model. Earth Syst.*, 8, 1552– 1564.
816 [doi:10.1002/2016MS000725](https://doi.org/10.1002/2016MS000725).
- 817 Han, J., M.L. Witek, J. Teixeira, R. Sun, H. Pan, J.K. Fletcher, and C.S. Bretherton. (2016).
818 Implementation in the NCEP GFS of a hybrid eddy-diffusivity mass-flux (EDMF) boundary
819 layer parameterization with dissipative heating and modified stable boundary layer mixing. *Wea.*
820 *Forecasting*, 31, 341–352. <https://doi.org/10.1175/WAF-D-15-0053.1>
- 821 Han, J., & Pan, H.-L. (2011). Revision of convection and vertical diffusion schemes in the NCEP
822 Global Forecast System. *Weather and Forecasting*, 26(4), 520–533.

- 823 Han, J., Wang, W., Kwon, Y. C., Hong, S.-Y., Tallapragada, V., & Yang, F. (2017). Updates in
 824 the NCEP GFS cumulus convection schemes with scale and aerosol awareness. *Weather and*
 825 *Forecasting*, *32*, 2005–eeting2017.
- 826 Harris, L. M., & Lin, S. J. (2013). A two-way nested global-regional dynamical core on the
 827 cubed-sphere grid. *Monthly Weather Review*, *141*(1), 283-306.
- 828 Harris, L., Lin, S. J., & Chen, J. H. (2014, May). Great Plains warm-season precipitation in a
 829 two-way nested high-resolution GCM. In *EGU General Assembly Conference Abstracts* (Vol.
 830 16).
- 831 Harris, L. M., Lin, S. J., & Tu, C. (2016). High-resolution climate simulations using GFDL
 832 HiRAM with a stretched global grid. *Journal of Climate*, *29*(11), 4293-4314.
- 833 Harris, L. M., Rees, S. L., Morin, M., Zhou, L., & Stern, W. F. (2019). Explicit Prediction of
 834 Continental Convection in a Skillful Variable-Resolution Global Model. *Journal of Advances in*
 835 *Modeling Earth Systems*, *11*(6), 1847-1869.
- 836 Hazelton, A. T., Bender, M., Morin, M., Harris, L., & Lin, S. J. (2018). 2017 Atlantic hurricane
 837 forecasts from a high-resolution version of the GFDL fvGFS model: Evaluation of track,
 838 intensity, and structure. *Weather and Forecasting*, *33*(5), 1317-1337.
- 839 Hazelton, A. T., Harris, L., & Lin, S. J. (2018). Evaluation of tropical cyclone structure forecasts
 840 in a high-resolution version of the multiscale GFDL fvGFS model. *Weather and*
 841 *Forecasting*, *33*(2), 419-442.
- 842 Hazelton, A., et al. (2020). The Global-Nested hurricane analysis and forecast system (HAFS):
 843 results from the 2019 Atlantic hurricane season. In *100th Annual Meeting*. AMS.
- 844 Held, I. M., Guo, H., Adcroft, A., Dunne, J. P., Horowitz, L. W., Krasting, J., ... & Wittenberg,
 845 A. T. (2019). Structure and performance of GFDL's CM4. 0 climate model. *Journal of Advances*
 846 *in Modeling Earth Systems*, *11*(11), 3691-3727.
- 847 Held, I. M., Zhao, M., & Wyman, B. (2007). Dynamic radiative-convective equilibria using
 848 GCM column physics. *Journal of the Atmospheric Sciences*, *64*(1), 228-238.
- 849 Hogan, R. J., & Mason, I. B. (2011). Deterministic forecasts of binary events. *Forecast*
 850 *verification: A practitioner's guide in atmospheric science*, 31-59.
- 851 Hong, S. Y., Noh, Y., & Dudhia, J. (2006). A new vertical diffusion package with an explicit
 852 treatment of entrainment processes. *Monthly weather review*, *134*(9), 2318-2341.
- 853 Hong, S.-Y. (2010). A new stable boundary-layer mixing scheme and its impact on the simulated
 854 East Asian summer monsoon. *Quarterly Journal of the Royal Meteorological Society*, *136*,
 855 1481–1496.
- 856 Jeevanjee, N. (2017). Vertical velocity in the gray zone. *Journal of Advances in Modeling Earth*
 857 *Systems*, *9*(6), 2304-2316.

- 858 Kim, H., F. Vitart, and D.E. Waliser. (2018). Prediction of the Madden–Julian Oscillation: A
 859 *Review. J. Climate*, 31, 9425–9443. <https://doi.org/10.1175/JCLI-D-18-0210.1>
- 860 Klingaman, N. P., & Demott, C. A. (2020). Mean-state biases and interannual variability affect
 861 perceived sensitivities of the Madden–Julian oscillation to air–sea coupling. *Journal of Advances*
 862 *in Modeling Earth Systems*, 12, e2019MS001799. <https://doi.org/10.1029/2019MS001799>
- 863 Knutson, T. R., Sirutis, J. J., Garner, S. T., Held, I. M., & Tuleya, R. E. (2007). Simulation of the
 864 recent multidecadal increase of Atlantic hurricane activity using an 18-km-grid regional
 865 model. *Bulletin of the American Meteorological Society*, 88(10), 1549-1565.
- 866 Knutson, T. R., & Tuleya, R. E. (2008). *Tropical cyclones and climate change: revisiting recent*
 867 *studies at GFDL* (pp. 120-144). Cambridge, UK: Cambridge University Press.
- 868 Krueger, S. K., Fu, Q., Liou, K. N., & Chin, H. N. S. (1995). Improvements of an ice-phase
 869 microphysics parameterization for use in numerical simulations of tropical convection. *Journal*
 870 *of Applied Meteorology*, 34(1), 281-287.
- 871 Landsea, C.W. and J.L. Franklin. (2013). Atlantic Hurricane Database Uncertainty and
 872 Presentation of a New Database Format. *Mon. Wea. Rev.*, 141, 3576–
 873 3592. <https://doi.org/10.1175/MWR-D-12-00254.1>
- 874 Lin, Y. L., Farley, R. D., & Orville, H. D. (1983). Bulk parameterization of the snow field in a
 875 cloud model. *Journal of climate and applied meteorology*, 22(6), 1065-1092.
- 876 Lin, S. J. (2004). A "vertically Lagrangian" finite-volume dynamical core for global
 877 models. *Monthly Weather Review*, 132(10), 2293-2307.
- 878 Lin, S. J. (2013). From Large-Eddy-Simulation to climate modeling: GFDL's unified global-
 879 regional non-hydrostatic modeling framework. In *Tropical Cyclone Research Forum: 67th IHC*
 880 *Presentations*.
- 881 Lin, S.-J., Harris, L. M., Benson, R., Zhou, L., Chen, J.-H., & Chen, X. (2017). Towards a
 882 unified prediction system from weather to climate scale. Second Symposium on Multi-Scale
 883 Atmospheric Predictability, Seattle, WA, Paper 3.1.
- 884 Lord, S., Willoughby, H. E., & Piotrowicz, J. M. (1984). Role of a parameterized ice-phase
 885 microphysics in an axisymmetric, nonhydrostatic tropical cyclone model. *Journal of the*
 886 *Atmospheric Sciences*, 41(19), 2836-2848.
- 887 Marchok, T. (2018, April). Factors Important for Tropical Cyclone Tracking in NWP Output.
 888 In *33rd Conference on Hurricanes and Tropical Meteorology*. AMS.
- 889 Marchok, T., Morin, M. J., Knaff, J., Sampson, C. R., Hazelton, A., & Lin, S. J. (2018, April).
 890 An Evaluation of Surface Wind Structure Forecasts from the fvGFS and Operational Dynamical
 891 Models. In *33rd Conference on Hurricanes and Tropical Meteorology*. AMS.

- 892 McCormack, J. P., Eckermann, S. D., Siskind, D. E., and McGee, T. J. (2006). CHEM2D-OPP:
893 A new linearized gas-phase ozone photochemistry parameterization for high-altitude NWP and
894 climate models, *Atmos. Chem. Phys.*, 6, 4943–4972. <https://doi.org/10.5194/acp-6-4943-2006>.
- 895 McGregor, J.L. (2015). Recent developments in variable-resolution global climate
896 modelling. *Climatic Change*, 129, 369–380. <https://doi.org/10.1007/s10584-013-0866-5>
- 897 NCEP (2020). List of GFS Implementations. Available at
898 [https://www.emc.ncep.noaa.gov/emc/pages/numerical_forecast_systems/gfs/implementations.ph](https://www.emc.ncep.noaa.gov/emc/pages/numerical_forecast_systems/gfs/implementations.php)
899 [p](https://www.emc.ncep.noaa.gov/emc/pages/numerical_forecast_systems/gfs/implementations.php) . Last accessed 22 May 2020.
- 900 Pauluis, O., & Garner, S. (2006). Sensitivity of radiative–convective equilibrium simulations to
901 horizontal resolution. *Journal of the atmospheric sciences*, 63(7), 1910–1923.
- 902 Pollard, R. T., Rhines, P. B., & Thompson, R. (1973). The deepening of the mixed layer.
903 *Geophysical Fluid Dynamics*, 3, 381–404.
- 904 Potvin, C.K., J.R. Carley, A.J. Clark, L.J. Wicker, P.S. Skinner, A.E. Reinhart, B.T. Gallo, J.S.
905 Kain, G.S. Romine, E.A. Aligo, K.A. Brewster, D.C. Dowell, L.M. Harris, I.L. Jirak, F. Kong,
906 T.A. Supinie, K.W. Thomas, X. Wang, Y. Wang, and M. Xue. (2019). Systematic Comparison
907 of Convection-Allowing Models during the 2017 NOAA HWT Spring Forecasting Experiment.
908 *Wea. Forecasting*, 34, 1395–1416. <https://doi.org/10.1175/WAF-D-19-0056.1>
- 909 Putman, W M., and Shian-Jiann Lin (2007). Finite-volume transport on various cubed-sphere
910 grids. *Journal of Computational Physics*, 227(1), 55–78.
- 911 Putman, W. M., & Suarez, M. (2011). Cloud-system resolving simulations with the NASA
912 Goddard Earth Observing System global atmospheric model (GEOS-5). *Geophysical Research*
913 *Letters*, 38(16).
- 914 Putman, W. M., & Suárez, M. J. (2017). GEOS Atmospheric Model: Challenges at Exascale.
- 915 Roberts, N.M. and H.W. Lean. (2008). Scale-Selective Verification of Rainfall Accumulations
916 from High-Resolution Forecasts of Convective Events. *Mon. Wea. Rev.*, 136, 78–97.
917 <https://doi.org/10.1175/2007MWR2123.1>
- 918 Satoh, M. (2007). Global Cloud-Resolving Model Development and its seamless Applications to
919 Weather & Climate Researches. In *Abstract Collection of the Third China-Korea-Japan Joint*
920 *Conference on Meteorology*.
- 921 Satoh, M., Stevens, B., Judt, F., Khairoutdinov, M., Lin, S. J., Putman, W. M., & Düben, P.
922 (2019). Global cloud-resolving models. *Current Climate Change Reports*, 5(3), 172–184.
- 923 Sela, J. G. (2010). The derivation of the sigma pressure hybrid coordinate Semi-Lagrangian
924 model equations for the GFS.
- 925 Shevliakova, E., and coauthors. (2020). The land component LM4.1 of the GFDL Earth System
926 Model ESM4.1: biophysical and biogeochemical processes and interactions with climate.
927 Submitted to *J. Adv. Modeling Earth Sys.*

- 928 Snook, N., Kong, F., Brewster, K. A., Xue, M., Thomas, K. W., Supinie, T. A., ... & Albright, B.
929 (2019). Evaluation of convection-permitting precipitation forecast products using WRF, NMMB,
930 and FV3 for the 2016–17 NOAA Hydrometeorology Testbed Flash Flood and Intense Rainfall
931 Experiments. *Weather and Forecasting*, *34*(3), 781–804.
- 932 Sobash, R.A., J.S. Kain, D.R. Bright, A.R. Dean, M.C. Coniglio, and S.J. Weiss. (2011).
933 Probabilistic Forecast Guidance for Severe Thunderstorms Based on the Identification of
934 Extreme Phenomena in Convection-Allowing Model Forecasts. *Wea. Forecasting*, *26*, 714–728.
935 <https://doi.org/10.1175/WAF-D-10-05046.1>
- 936 Sobash, R.A., G.S. Romine, C.S. Schwartz, D.J. Gagne, and M.L. Weisman. (2016). Explicit
937 Forecasts of Low-Level Rotation from Convection-Allowing Models for Next-Day Tornado
938 Prediction. *Wea. Forecasting*, *31*, 1591–1614. <https://doi.org/10.1175/WAF-D-16-0073.1>
- 939 Sobash, R.A., C.S. Schwartz, G.S. Romine, and M.L. Weisman. (2019). Next-Day Prediction of
940 Tornadoes Using Convection-Allowing Models with 1-km Horizontal Grid Spacing. *Wea.*
941 *Forecasting*, *34*, 1117–1135. <https://doi.org/10.1175/WAF-D-19-0044.1>
- 942 Thiébaux, J., E. Rogers, W. Wang, and B. Katz. (2003). A New High-Resolution Blended Real-
943 Time Global Sea Surface Temperature Analysis. *Bull. Amer. Meteor. Soc.*, *84*, 645–
944 656. <https://doi.org/10.1175/BAMS-84-5-645>
- 945 Van Leer, B. (1974). Towards the ultimate conservative difference scheme. II. Monotonicity and
946 conservation combined in a second-order scheme. *Journal of computational physics*, *14*(4), 361-
947 370.
- 948 Vecchi, G. A., Murakami, H., Delworth, T. L., Underwood, S., Wittenberg, A. T., Zeng, F. J., ...
949 & Kapnick, S. B. (2019). Tropical cyclone sensitivity to global forcing: seeds and
950 probability. *AGUFM*, 2019, A32F-06.
- 951 Vitart, F., Ardilouze, C., Bonet, A., Brookshaw, A., Chen, M., Codorean, C., ... & Hendon, H.
952 (2017). The subseasonal to seasonal (S2S) prediction project database. *Bulletin of the American*
953 *Meteorological Society*, *98*(1), 163–173.
- 954 Wei, H., Zheng, W., Meng, J., Gayno, G., Hou, Y., & Ek, M. (2017). Planned land surface
955 changes for the next NEMS implementation. In *28th Conf. on Weather Analysis and*
956 *Forecasting/ 24th Conf. on Numerical Weather Prediction*, American Meteorological Society,
957 Seattle, WA, pp. 600.
- 958 Wheeler, M. C., & Hendon, H. H. (2004). An all-season real-time multivariate MJO index:
959 Development of an index for monitoring and prediction. *Monthly weather review*, *132*(8), 1917-
960 1932.
- 961 Wilson, T. H., and R. G. Fovell. (2018). Modeling the evolution and life cycle of radiative cold
962 pools and fog. *Weather and Forecasting*, *33*, 2031–220.
- 963 Xiang, B., Zhao, M., Jiang, X., Lin, S. J., Li, T., Fu, X., & Vecchi, G. (2015). The 3–4-week
964 MJO prediction skill in a GFDL coupled model. *Journal of Climate*, *28*(13), 5351–5364.

- 965 Xu, K.-M., & Randall, D. A. (1996). A semiempirical cloudiness parameterization for use in
966 climate models. *Journal of the atmospheric sciences*, 53(21), 3084–3102.
- 967 Yoneyama, K., C. Zhang, and C.N. Long. (2013). Tracking Pulses of the Madden–Julian
968 Oscillation. *Bull. Amer. Meteor. Soc.*, 94, 1871–1891. <https://doi.org/10.1175/BAMS-D-12-00157.1>
- 970 Zhang, C., Xue, M., Supinie, T. A., Kong, F., Snook, N., Thomas, K. W., et al. (2019). How well
971 does an FV3-based model predict precipitation at a convection-allowing resolution? Results from
972 CAPS forecasts for the 2018 NOAA hazardous weather test bed with different physics
973 combinations. *Geophysical Research Letters*, 46, 3523–
974 3531. <https://doi.org/10.1029/2018GL081702>
- 975 Zhang, J.A., D.S. Nolan, R.F. Rogers, and V. Tallapragada. (2015). Evaluating the Impact of
976 Improvements in the Boundary Layer Parameterization on Hurricane Intensity and Structure
977 Forecasts in HWRF. *Mon. Wea. Rev.*, 143, 3136–3155. <https://doi.org/10.1175/MWR-D-14-00339.1>
- 979 Zhao, M., Golaz, J. C., Held, I. M., Ramaswamy, V., Lin, S. J., Ming, Y., ... & Guo, H. (2016).
980 Uncertainty in model climate sensitivity traced to representations of cumulus precipitation
981 microphysics. *Journal of Climate*, 29(2), 543-560.
- 982 Zhao, M., Golaz, J.-C., Held, I. M., Guo, H., Balaji, V., Benson, R., et al. (2018). The GFDL
983 global atmosphere and land model AM4.0/LM4.0: 1. Simulation characteristics with prescribed
984 SSTs. *Journal of Advances in Modeling Earth Systems*, 10, 691–734.
985 <https://doi.org/10.1002/2017MS001208>
- 986 Zhao, M., Held, I. M., Lin, S. J., & Vecchi, G. A. (2009). Simulations of global hurricane
987 climatology, interannual variability, and response to global warming using a 50-km resolution
988 GCM. *Journal of Climate*, 22(24), 6653-6678.
- 989 Zhao, Q., & Carr, F. H. (1997). A prognostic cloud scheme for operational NWP
990 models. *Monthly Weather Review*, 125(8), 1931–1953.
- 991 Zhou, L., Lin, S.-J., Chen, J.-H., Harris, L. M., Chen, X., & Rees, S. L. (2019). Toward
992 convective-scale prediction within the next generation global prediction system. *Bulletin of the*
993 *American Meteorological Society*. <https://doi.org/10.1175/BAMS-D-17-0246.1>
- 994